

Jimma University  
Jimma Institute of Technology  
Faculty of Mechanical Engineering  
Thermal System Engineering

**DESIGN AND COMPUTATIONAL FLUID DYNAMICS MODELING  
OF ULTRA-LOW HEAD DUAL AXIS CROSS FLOW TURBINE:  
WONJI-SHOA SUGAR FACTORY IRRIGATION CANAL FLOW IN  
FOCUS**

A Thesis Submitted to the School of Postgraduate Studies of Jimma Institute of Technology,  
Faculty of Mechanical Engineering in Partial Fulfilment of the Requirements for the Degree of  
Master of Science in Thermal System Engineering.

By: Surafel Kifle

Jimma, Ethiopia

July 2019

Jimma University  
Jimma Institute of Technology  
Faculty of Mechanical Engineering  
Thermal System Engineering

**DESIGN AND COMPUTATIONAL FLUID DYNAMICS MODELING  
OF ULTRA-LOW HEAD DUALAXIS CROSS FLOWTURBINE:  
WONJI-SHOASUGAR FACTORY IRRIGATION CANAL FLOWIN  
FOCUS**

A Thesis Submitted to the School of Postgraduate studies of Jimma Institute of Technology,  
Faculty of Mechanical Engineering in Partial Fulfilment of the Requirements for the Degree of  
Master of Science in Thermal System Engineering.

By:Surafel Kifle

**Principal Advisor:**Balewgize Amare Zeru (Asst. Prof.,Ph.D. Candidate)

**Co - Advisor:**Nebiyu Bogale Mereke (M.Sc., Asst. Prof.,)

Jimma, Ethiopia

July 2019

## DECLARATION

I, the under signed, declare that this thesis entitled “Design and Computational Fluid Dynamics Modeling of Ultra-Low Head Dual Axis Cross Flow Turbine: Wonji-ShoaSugar Factory Irrigation CanalFlow in focus” is my original work, and has not been presented by any other person for an award of a degree in this or any other University.

Surafel Kifle	_____	_____
<b>Student Name</b>	Signature	Date

This thesis has been submitted for examination with my approval as university supervisor.

Balewgize Amare Zeru (Asst. Prof,Ph.D.fellow)	_____	_____
<b>Principal Advisor</b>	Signature	Date

Nebiyu Bogale (M.Sc., Asst. Prof.)	_____	_____
<b>Co Advisor</b>	Signature	Date

Solomon Tesfamariam(PhD)	_____	_____
<b>External Examiner</b>	Signature	Date

Fikadu Kifle (M.Sc)	_____	_____
<b>Internal Examiner</b>	Signature	Date

Fikadu Kifle (M.Sc.)	_____	_____
<b>Chair Man</b>	Signature	Date

## **ACKNOWLEDGEMENTS**

First, I would like to thank the merciful and almighty God who made possible for me to begin and finish this work successfully.

Second, I take great pleasure in acknowledging my advisors Balewgize Amare Zeru (Asst.Prof.,Ph.D. fellow at Otto von Guericke University ofMagdeburg, Germany) and Nebiyu Bogale (MSc., Asst.Prof. of Mechanical Engineering)for their great encouragement, insightfulcomments, and continuous support throughout the process of this thesis accomplishment.Next, my sincere thanks also goes to Abiyou Solomon(MSc., Ph.D.fellow at Otto von Guericke University ofMagdeburg, Germany) forproviding me valuable and intellectual guidance on speed multiplier design used in a cross flow turbine to increase rotational speed from a lower-speed turbine runner to a higher speed electrical generator.

Third, I would like to gratitude Jimma University (Jimma Institution of Technology) and Faculty of Mechanical Engineering for sponsoring my MSc. Program in Thermal System Engineering.

Last but not the least, I would like to express my humble respect and special thanks to my parents and others who has directly or indirectly helped me during this thesis work.

## ABSTRACT

*In Ethiopia, the main source of power supply is large scale hydropower plants, which accounts a total generation of 3,822MW in 2019. However, there are a number of problems associated with power transmission schemes for rural electrification. Therefore, this thesis is focused on the design and Computational Fluid Dynamics(CFD) Modelling of Ultra-Low Head (ULH) dual axis cross flow turbine focusing on Wonji-Shoa sugar factory irrigation canal flow. To this end, a design having two measure phases, analytical and CFD analysis, was adopted. The analytical phase includes three sub-components namely, turbine runner, nozzle and speed multiplier mechanism. The analytical design process starts with calculation of initial dimension for the turbine runner based up on various, relevant literatures reviewed. Similarly, the CFD analysis phase focused on developing a methodology used for the CFD analysis, visualization of the results and predicting the performance of ULH turbine. The 3D geometry was also designed on ANSYS design modeler. Subsequently, the model was imported and simulation was performed by using the commercial software ANSYS Fluent 18.0 version. Moreover, a procedure for CFD simulation was followed and physical assumptions were taken based on the literatures reviewed. Finally, the velocity and pressure distribution within the internal surface nozzle, turbine casing, and runner of the cross-flow turbine were analyzed. Accordingly, the simulation results disclosed that the turbine efficiency was improved from 67.5% to 78% (increase by 10.5%) numerically. In other words, when the rotational speed of the turbine is increased from 375 to 650 rpm, the efficiency is increased by 10.5% higher than the design rotational speed of 375rpm. From the results of the simulation, it was also observed that the efficiency will decrease if the rotational speed goes beyond 650 rpm. The overall result depict that the turbine efficiency obtained from the CFD analysis and analytical approaches were found as 78 % and 87.9%, respectively. In line with the findings, future recommendations were also suggested to pave the way for further improvement on the design of this study.*

**Keywords:** *Renewable Energy, Turbomachinery, Micro Hydropower, Ultra-low Head Turbine, Speed multiplier mechanism, Computational Fluid Dynamics, ANSYS Fluent, Efficiency.*

**TABLE OF CONTENTS**

ACKNOWLEDGEMENTS .....	i
ABSTRACT .....	ii
LIST OF FIGURES .....	vii
NOMENCLATURE .....	ix
ABBREVIATIONS .....	xii
CHAPTER 1. INTRODUCTION .....	1
1.1. Background.....	1
1.2. Hydro-power Classification by Size .....	3
1.3. Importance of Micro Hydropower.....	3
1.3.1 Increased Productivity .....	4
1.3.2. Environmental Considerations .....	4
1.3.3. Social Considerations .....	5
1.4. Description of Cross Flow Turbine .....	5
1.5. A cross flow turbine consists of the following components .....	6
1.6. Statement of the Problem.....	6
1.7. Objectives .....	7
1.7.1. General Objective .....	7
1.7.2. Specific Objectives.....	7
1.8. Scope of the Study.....	8
1.9. Expected outcome.....	8
1.10. Description of the Study Area .....	8
1.11. Significance of the study .....	9
1.12. Study methodology .....	9
1.13. Structure of the Thesis .....	10
CHAPTER 2. LITERATURE REVIEW .....	11
2.1. General Description of Hydropower.....	11
2.2. Hydropower classification by type.....	12
2.2.1. Storage Hydropower (Conventional Plant) .....	12
2.2.2. Pumped Storage plant (PSP).....	13
2.2.3. Run-of-the-River hydropower plants.....	14

2.3. Types of Water Turbines .....	15
2.4. Reaction Turbine.....	17
2.5. Impulse Turbine .....	18
2.6. Review of previous studies related with the study topic .....	20
2.7. Scientific Gap.....	24
CHAPTER 3. DESIGN OF CROSS FLOW TURBINE COMPONENTS .....	25
3.1. Site Data.....	25
3.2. Design Profile of Nozzle .....	25
3.2.1. Bernoulli's Principle .....	25
3.2.2. The Linear Momentum.....	29
3.2.3. Flow Controlling Mechanism.....	30
3.3. Determination of Potential Power and Efficiency of Cross Flow Turbine.....	30
3.3.1. Hydraulic Power Input due to Head: .....	30
3.3.2. The Velocity Triangle of Cross Flow Turbine .....	31
3.3.3. Theoretical Power Output:.....	32
3.3.4. Calculating Theoretical Efficiency of Ultra-Low Head Cross Flow Turbine: .....	33
3.4. Theoretical Design of Cross Flow Turbine Runner .....	34
3.4.1. Calculating Rotational Speed of Turbine: .....	34
3.5. Design of Blade Angle and Blade Velocity of Cross Flow Turbine.....	38
3.6. Theoretical Torque and Force Transferred in the Two Stages .....	40
3.6.1. Percentages of Power Produced from Both Stages .....	41
3.7. Design of Speed Multiplying Mechanism.....	42
3.7.1. Basic Geometry of Spur Gears .....	43
3.7.2. Design of One Stage Spur Gear Speed Multipliers .....	43
3.7.2.5. Estimation of Module based on Beam Strength .....	46
3.8. Checking for Design of Pinion Gear:.....	47
3.8.1. Design based on Contact Strength.....	47
3.8.2. Design for Pinion based on Bending Stress.....	48
3.8.3. Design for Pinion Based on Dynamic Load .....	48
3.9. Design Based on Wear strength.....	49
3.9.1. Calculation of the Maximum Wear Load for Pinion.....	49

3.10. Checking for Design of Larger Gear: .....	49
3.10.1. Design for Gear Based on Induced Bending Stress.....	49
3.10.2. Design for Gear Based on Induced Contact Stress.....	49
3.10.3. Design for Gear Based on Dynamic Load.....	50
3.10.4. Calculation of the Maximum Wear Load for Gear.....	50
CHAPTER 4.COMPUTATIONAL FLUID DYNAMICS MODELING OF TURBINE .....	51
4.1. Introduction to Computational Fluid Dynamics .....	51
4.2. Computational Fluid Dynamics Analysis in Hydraulic Turbine Design .....	52
4.3. Limitations of Computational Fluid Dynamics Methodology.....	53
4.4. Governing Equations and their Discretization.....	53
4.5. Governing Equations of Fluid Flow.....	54
4.5.1. Principle of Conservation of Mass: .....	54
4.5.2. Principle of Conservation of Momentum .....	54
4.5.3. Principle of Conservation of Energy: .....	55
4.6. Discretization Method.....	55
4.6.1. Finite Difference Method .....	55
4.6.2. Finite Element Method .....	56
4.6.3. Finite Volume Method.....	56
4.7. Numerical Grid Generation .....	57
4.7.1. Structured (regular) Grid .....	57
4.7.2. Unstructured Grid .....	57
4.8. Pre-processing .....	57
4.9. Convergence Criteria.....	58
4.10. Post-Processing the Results.....	58
4.11. Torque and Efficiency.....	58
4.12. Computational Fluid Dynamics Simulation Methodology .....	59
4.12.1. Geometrical Modeling.....	59
4.12.2. Computational Mesh Generation.....	61
4.12.3. Problem Solving Setup .....	63
4.12.5. Solution Method .....	68
4.12.6. Solver Control.....	68



---

4.12.7. Solution Initialization .....	69
CHAPTER 5 RESULTS AND DISCUSSION.....	70
5.1. General .....	70
5.2. Graphical Display .....	70
5.2.1. Pressure Distribution on the Cross Flow Turbine .....	70
5.2.2. Velocity Vectors and Velocity Distributions.....	72
5.3. The Numerical Hydraulic Efficiency Comparison.....	73
CHAPTER 6 CONCLUSIONS AND RECOMMENDATIONS .....	75
6.1. Conclusions .....	75
6.2. Recommendations .....	76
REFERENCES .....	77
APPENDIX.....	81
APPENDIX A.....	81
APPENDIX B .....	83

**LIST OF FIGURES**

Figure 1: Global share of renewable energy .....	2
Figure 2: Schematic sketch of the model cross flow turbine .....	5
Figure 3: Map of study area .....	8
Figure 4: Flow chart of the study design .....	10
Figure 5: General scheme of reservoir hydropower plant .....	13
Figure 6: General scheme of pumped storage hydropower plant .....	14
Figure 7: General scheme of run of river hydropower plant .....	15
Figure 8: Different turbine application based on head and flow rate .....	15
Figure 9: Comparison of typical efficiencies of different turbines .....	16
Figure 10: Reaction turbines .....	17
Figure 11: Pelton turbine side view with fixed nozzle .....	18
Figure 12: Water jet impingement on the turgo runner .....	19
Figure 13: Cross flow turbine .....	19
Figure 14: Theoretical velocity triangles of a cross- flow turbine runner .....	31
Figure 15: Runner blade profile .....	37
Figure 16: Basic gear geometry .....	43
Figure 17: the 3d geometry of dual axis cross flow .....	60
Figure 18: The 3D geometry for numerical analysis .....	61
Figure 19: Computational mesh of the rotating domains .....	62
Figure 20: Mesh of the stationary domain with nozzle inlet face .....	63
Figure 21: Selection of material .....	64
Figure 22: Selection of turbulence model .....	64
Figure 23: Cell zone condition for runner .....	65
Figure 24: Inlet velocity boundary condition panel .....	66
Figure 25: Outlet pressure boundary condition panel .....	67
Figure 26: Boundary condition for runner wall .....	68
Figure 27: The contours of static pressure .....	71
Figure 28: Displays the total pressure contours on the blades .....	71
Figure 29: Velocity distribution of cross flow turbine .....	72
Figure 30: Furbine performance curves as a function of rotational speed .....	73

**LIST OF TABLES**

Table 1: World shp by region (< 10 mw) ..... 2

Table 2: Classification of small hydro power schemes ..... 3

Table 3: Classification of small hydro based on head ..... 3

Table 4: Selection of generator type ..... 20

Table 5: Material specifications ..... 44

Table 6: Theoretical calculations of conventional spur gear ..... 47

## NOMENCLATURE

$A_{in}$	Water inlet cross section area of the nozzle	[m <sup>2</sup> ]
$A_{out}$	Water outlet cross section area of the nozzle	[m <sup>2</sup> ]
$B_2$	Outlet of the nozzle depth,	[m]
$D_{in}$	Runner inner diameter	[m]
$D_o$	Runner outer diameter	[m]
$F_{dg}$	Dynamic load on the gear tooth,	[kN]
$F_{dp}$	Dynamic load on the pinion gear tooth	[kN]
$F_N$	External force acting on the nozzle	[kN]
$F_p$	Force of pressure distribution to the inside the nozzle	[kN]
$g$	Acceleration due to gravity	[m/s <sup>2</sup> ]
$H_{gross}$	Gross head	[m]
$H_{Losses}$	Head loss,	[m]
$H_{net}$	Net head	[m]
$h_1$	Height of nozzle inlet	[m]
$h_2$	Outlet height of the nozzle	[m]
$L$	Runner Length	[m]
$l$	Length of the rectangular nozzle	[m]
$M_T$	Normal twisting moment	[N-m]
$N_G$	Angular velocity of drive gear	[rpm]
$N_P$	Angular velocity of driver gear	[rpm]
$n$	Number of blades	[-]
$P_{atm}$	Atmospheric pressure	[N/mm <sup>2</sup> ]
$P_1$	Total pressure at the inlet of the nozzle	[N/mm <sup>2</sup> ]
$P_2$	Total pressure at the exit of the runner	[N/mm <sup>2</sup> ]
$Q$	Total flowrate in the system	[m <sup>3</sup> /s]
$R_c$	Radius of blade curvature	[m]
$S_1$	Blade thickness	[m]
$N_s$	Specific speed of turbine	[rpm]
$t_b$	Blade spacing	[m]

---

T	Torque	[Nm]
$t_j$	Thickness of the jet water entrance	[m]
U	Peripheral velocity	[m/s]
V	Pitch line Velocity	[m/s]
$V_1$	Absolute Velocity of the first stage inlet	[m/s]
$V_2$	Absolute Velocity of the first stage exit	[m/s]
$V_3$	Absolute Velocity of the second stage inlet	[m/s]
$V_4$	Absolute Velocity of the second stage exit	[m/s]
$V_B$	Discharge velocity of water in to the nozzle	[m/s]
$V_1$	Initial velocity of fluid	[m/s]
$V_2$	Exit velocity of fluid	[m/s]
$V_{in}$	Inlet velocity of water	[m/s]
$V_{r1}$	Runner inlet relative velocity	[m/s]
$V_{r2}$	Runner outlet relative velocity	[m/s]
$V_{out}$	Outlet velocity of water	[m/s]
$V_{\omega 2}$	Exit elocity of Whirl	[m/s]
$V_{\omega 1}$	Inlet elocity of Whirl	[m/s]
$P_t$	Turbine power output	[kw]
Y	Lewis form factor	[-]
$Z_G$	Number pf teeth on drive	[-]

**-Greek symbols**

$\alpha$	Angle of attack	[°]
$\Delta\omega$	Change of the Velocity of Whirl	[m/s]
$\rho$	Density of water	[kg/m <sup>3</sup> ]
$\phi$	Pressure angle	[°]
$\psi$	Relative Velocity factor	[-]
$\beta_1$	Blade inlet angle	[°]
$\beta_2$	Blade inlet angle	[°]
$\eta$	Efficiency of turbine	[%]
$\theta$	Blade central angle	[°]

**ABBREVIATIONS**

ANSYS	ANalysis SYStems
CFD	Computational Fluid Dynamics
CFT	Cross Flow Turbine
EEPCo	Ethiopian Electric Power Corporation
FEM	Finite Element Method
FDM	Finite Difference method
FVM	Finite Volume Method
HPPs	Pumped storage hydro power plants
Kw	Kilo-Watt
MW	Mega Watt
MHP	Micro-Hydropower Plant
RANS	Reynolds-averaged Navier –Stokes
RPM	Revolution per Minute
SHP	Small Hydro Power
SST	Shear Stress Transport
ULH	Ultra-Low Head

## **CHAPTER 1. INTRODUCTION**

### **1.1. Background**

Renewable energy provides one of the most effective strategies to simultaneously promote clean development, sustainable access and energy security with its irreplaceable role in climate change mitigation at all levels. Today, more than two-thirds of the world's renewable electricity comes from hydropower [1]. In both developing and developed countries, the need for clean and sustainable sources of energy is growing more acute in the face of climate change while geopolitical and economic uncertainty over traditional fossil-fuel markets highlights the importance of energy diversification and independence. On the other hand, the number of population, their demand, and activities are increased; an unsustainable consumption and production patterns have resulted in economic and social costs that may affect the human life and the natural resources as well. The global communities consume electricity from the main sources that are fossil fuel, hydropower, nuclear, biomass, wind, geothermal and solar taking accounts of 67.5 %, 16%, 13 %, 1.3%, 1.1%, 0.3 % and 0.07 % respectively in 2015 [2]. However, the major sources of electricity, fossil fuels take account to release more CO<sub>2</sub> gas, which contributes to increasing greenhouse gases in the atmosphere. As a result, in the form of global warming, the world temperature increases and then it affects not only life but also the sustainability of natural resources and ecosystems. Hence, the use of renewable energy sources can be an answer to the dual challenge of satisfying increasing energy needs and combating climate change. Renewable energy is available in different forms such as wind energy, solar energy, biomass energy, biogas energy, hydro and geothermal energy which are among the most important renewable sources for energy generation.

In a truly impulse turbine, all of the potential energy in water is converted into kinetic energy in the jet and the entire part of the runner is exposed to atmospheric pressure. It is the kinetic energy that is converted into the turbine shaft power. In a reaction turbine, both pressure energy and kinetic energy of the water are converted into shaft power. The turbine has to be filled with water at all time during its operation. In addition, there is significant pressure difference between the inlet and outlet of the turbine; the flow through the turbine depends on the speed and pressure across the turbine [3].



As one of the world’s most important renewable energy sources, SHP is fifth in development, with large hydropower having the highest installed capacity to date, followed by wind and solar power (Figure 1).

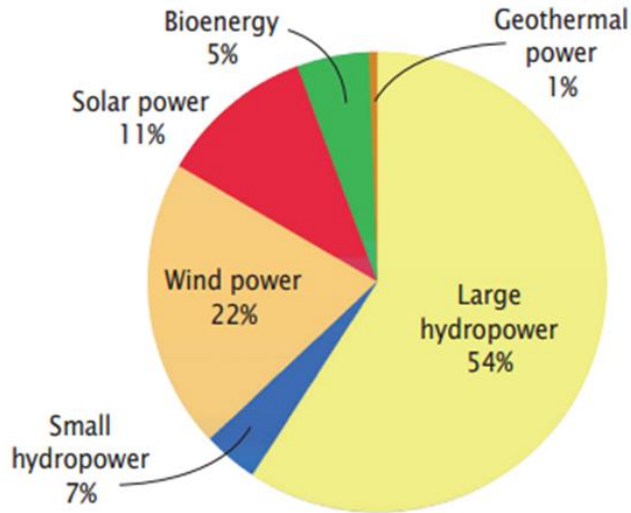


Figure 1:Global share of renewable energy [4].

Small, mini and micro hydro power plants have been in operation in Ethiopia since 1939. The first hydropower plant is the Aba Samuel hydropower plant with an installed capacity of 6 MW. Currently, an estimated potential of SHP is about more than 1,500MW that exists in Ethiopia. World installed capacity of small hydro power today is around 78GW against an estimated potential of 217GW. A general scenario of small hydro power potential and installed capacity worldwide is as under [4].

Table 1: World SHP by region (< 10 MW)[4]

COUNTRY	POTENTIAL SHP CAPACITY(MW)	INSTALLED SHP CAPACITY(MW)
Ethiopia	1,500	6
Africa	12,198	580
Europe	38,943	18,685
Asia	120,614	50,730
Oceania	1,206	447
America	86,868	14,702
TOTAL	259,829	85,144

### 1.2. Hydro-power Classification by Size

Generally, hydropower is usually classified by size (generating capacity) and the type of scheme (run-of-river, reservoir, pumped storage). The classification of small hydro power on the basis of capacity is shown in the following table 2.

Table 2: Classification of small hydro power schemes [5]

TYPE	POWER CAPACITY
Small Hydro	1-25000kw
Mini Hydro	100kw -1000kw
Micro Hydro	5-100kw

The classification of small hydro power on the basis of station capacity is shown in the following Table 3.

Table 3: Classification of small hydro based on head [6].

TYPE	RANGE OF HEAD
Ultra-Low Head	Below 3m
Low Head	3 to 40m
Medium/High head	Above 40m

### 1.3. Importance of MicroHydropower

Automatic isolated or autonomous small hydro power plants provide an alternative solution to electric grid extension that serves widely scattered communities, as a high efficiency power supplement to urban areas, small industries and for domestic purposes. Specifically, there is a great disparity between urban and isolated rural zones, with a consequent imbalance in the accessibility of energy. In most cases, the rural areas are far away from the national grid with bad terrain and without access roads. Therefore, it is unlikely that full rural electrification would be achieved through grid extension using sub-transmission lines from the National grid. However, in these same locations, there is abundant flowing water such as rivers, streams, waterfalls, and possibility of constructing irrigation canals, dams, etc. that in some cases can be easily exploited using small hydropower technologies.

In Ethiopia, most of the villages/towns are remotely located and interconnecting the grid system, if it has to transmit electricity to these villages/ towns, may not be that much technoeconomically viable. Presently, efforts are being made by Ethiopian Electric Power Corporation (EEPCo) through Universal Electric Access Program to electrify vast areas in Northern, Central, Southern, Western, and Eastern parts of the country. Although expansion of the national grid for rural electrification is progressing fast, there is still a vast possibility of developing micro hydro schemes, particularly, in those areas which are remotely located and are not covered presently under Universal Electric Access Program [7].

Nowadays, micro hydro is an important player in the remote, hilly and electrified areas of Ethiopia where there is a substantial potential that can be tapped. Therefore, micro hydro is one of the most valuable answers to the question of how to offer to isolated rural communities the benefits of electrification and the progress associated with it, as well as to improve the quality of life. Subsequently, benefits of small hydro include increased productivity, environmental and social advantages.

### **1.3.1 Increased Productivity**

Electricity can power home industries such as weaving and craft making and allow longer working hours through lighting. In the agricultural-industrial sector, the energy may be used for powering irrigation pumps, and for drying, harvesting and processing crops. Impressive gains in productivity can result from powering these types of tasks.

### **1.3.2. Environmental Considerations**

The current concern on the global environment has imposed a new constraint on the production of electricity. Small hydro stations are a renewable nonpolluting form of electricity generation; they require no fuel to produce energy and hence no emission. This is significant in light of concerns about pollution and of global warming arising from the burning of fossil fuels.

For example, the majority of China's hydro stations were built on the existing irrigation canal network. About 85% of the Ethiopian rural population where, along with cow dung, biogas and kerosene, wood is the principal fuel for cooking and heating; the use of electricity as an alternative energy source may slow deforestation and the resulting soil erosion, loss of nutrients and flooding.

### 1.3.3. Social Considerations

In rural areas, radio and television can be used to provide information on weather conditions, agriculture, and family planning. Electricity in schools can be used to power audio-visual teaching aids and to run laboratory equipment. It can also be used in rural health clinics for refrigeration of medical supplies. Electricity can enhance community life and help build institutions through its use in theatre, community meetings and adult education. Therefore, electrification can indirectly enhance rural development because electrified villages can provide better working and living conditions more attractive to doctors and other educated people. People with confidence in the survival of their community are more likely to work hard to strengthen it.

### 1.4. Description of Cross Flow Turbine

The Banki Turbine consists of two parts, a nozzle and a turbine runner. The runner is built up of two parallel circular disks joined together at the rim with a series of curved blades. The nozzle, whose cross-sectional area is rectangular, discharges the water jet through the full width of the wheel and enters the wheel at an angle of 16 degrees to the tangent of the periphery of the wheel. The main characteristic of the Cross-Flow turbine is the water jet of rectangular cross-section which passes twice through the rotor blades arranged at the periphery of the cylindrical rotor perpendicular to the rotor shaft. The water flows through the blades first from the periphery towards the center and then, after crossing the open space inside the runner, from the inside to outwards. Hence, energy conversion takes place twice: first upon impingement of water on the blades upon entry, and then when water strikes the blades upon exit from the runner [8].

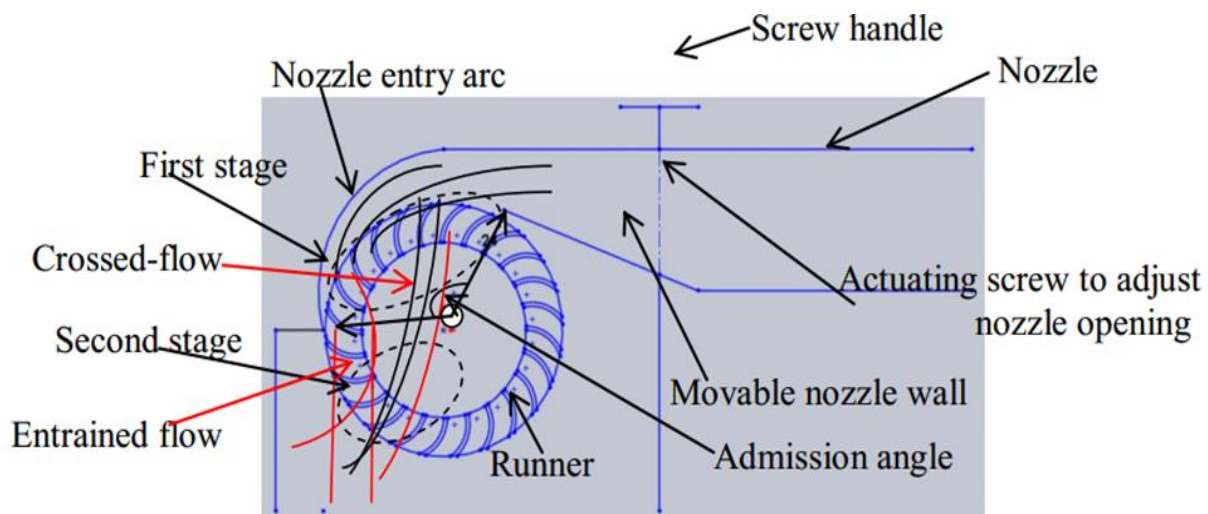


Figure 2: Schematic sketch of the model Cross flow turbine [8]

### **1.5.A cross flow turbine consists of the following components**

A). **Nozzle:** Cross flow turbine has one or more nozzles with rectangular cross-section to discharge water jet to the turbine. The main function of the nozzle is to convert the static energy of water to kinetic energy and simultaneously convey water to blades on the runner at the desired angle. Nozzle is mounted at the exit of the main pipeline and its exit is placed close to the outer periphery of the runner. The nozzle serves to change the incoming pressure into velocity.

B). **Runner with Blades:** Runner is the most important component of the turbine, where actual energy conversion takes place. Its design is critical for efficient performance of the turbine. It is equipped with curved blades fitted between runner discs. Blades are curved and mounted between two circular rims parallel to the axis of the shaft. Their function is to change smoothly the direction of the incoming flow from the nozzle.

C). **Casing:** Casing prevents splashing of water and directs the water to the draft tube, if present. Casing, in case of reaction turbine, creates near vacuum conditions for mounting the draft tube.

D). **Shaft and Bearings:** Shaft is an integral part of the runner. It transfers the torque generated by the turbine to the generator or alternator. Shaft should be designed correctly, so that it does not cause any hindrance to the flow of water to the second stage. The shaft is supported by bearings in order to reduce resistance to the rotation of the turbine.

E). **Draft Tube:** Draft tube connects the turbine outlet to the tailrace. It is used to recover a major portion of the residual energy left in the water escaping out of the runner. Moreover, it permits the turbine to be set above tailrace without any appreciable loss in head

G). **Guide Vanes:** Guide vanes direct the water and let it enter the runner smoothly, with minimum losses. In split cross flow turbine the admission of water into the runner is controlled by two guide vanes which divide the water flow. Both guide vanes can be adjusted independently and can be used as a shutoff valve or closing device if there is lower head.

### **1.6. Statement of the Problem**

In the 20<sup>th</sup> Century, renewable energy is not just an optional but a need because conventional energy sources decrease day by day and the global fossil fuel price raise every day. Continuous using of convectional energy sources have some impacts on human health and damages the forests, while electrical energy is an integral component of the overall development of any nation.

In Ethiopia, due to the highland topography and scattered settlement of the remote rural villages, extending the main grid line to this rural remote village becomes expensive. Due to this and other facts, about 85% of the Ethiopian rural population do not have access to electricity. Only communities living in urban area of Ethiopia have got the access of electricity, and most rural areas that are far from national grid are based on convectional energy resources, yet. On the other hand, more than 94% of Ethiopian energy consumption has been met through biomass fuels, such as wood, plant material or agricultural waste. Even though this is one of the renewable energy resources, if it is not used sustainably, it has severe effects on the environment and also for people.

A majority of rural household in Wonji-Shoa is not connected to the national grid. However, these villages do have existing irrigation canals constructed for sugar cane plantation. These canals can be suitable sites for micro hydropower (MHP). For these type of situation, ultra-low head (ULH) dual axis cross flow turbine that run at high flow rate and low head can be applicable. Recently, in Ethiopia there is no small hydropower plant designed in the energy recovery system from the existing irrigation system. In this regard, it is necessary to design ULH dual axis cross flow turbine can be a good idea for harnessing the water potential in sugar factory irrigation canal flow.

## **1.7. Objectives**

### **1.7.1. General Objective**

The main objective of study is design and computational fluid dynamics modelling of ultra-low head dual axis cross flow turbine: Wonji-Shoa Sugar Factory Irrigation canal flow in focus.

### **1.7.2. Specific Objectives**

To accomplish the present research, the following specific objectives were designed:

- ✓ Analyze the potential of power based on the measured flow rate and available head.
- ✓ Design of nozzle with rectangular cross-sectional area at the inlet and outlet which provide suitable jet speed for runners.
- ✓ Design of cross flow turbine runner based on the measured water flow rate and net head.
- ✓ Design speed multiplying mechanism that enables the alternator to provide energy.
- ✓ Computational Fluid Dynamics (CFD) simulation of the nozzle, turbine casing and runner.

### 1.8. Scope of the Study

The aim of this research is to analyze the potential of power based on the measured data, design of turbine runner, nozzle and speed multiplying mechanism and Computational Fluid Dynamics (CFD) modeling of turbine runner, nozzle, turbine casing are the scope of this study. Experimental/prototype development is not included in this study.

### 1.9. Expected outcome

After completion of the study, expected results are:

- Nozzle (for suitable water jet speed) and turbine runner will be designed.
- Suitable speed multiplying mechanism will be designed.
- Computational fluid dynamics modeling of turbine runner, nozzle and turbine casing will be performed.

### 1.10. Description of the Study Area

The present study was carried out in Wonji/Shoa irrigation canal. The Wonji–Shoa Sugar Estate lies downstream of the Koka Dam in the Central Rift Valley of Ethiopia in the Awash River Basin, 110 km southeast of Addis Ababa and 10 km south of Nazareth by road as shown in Figure 3. It is located at 8° 30' to 8° 35' N and 39° 10' to 39° 20' E at an altitude of 1540 meter above sea level. More than 50 percent of the farm is heavy clay soil and the rest is light soil. It has a semi-arid climate and receives an average annual rainfall of 831.2 mm, peak daily evapotranspiration of 4.5 mm, mean annual maximum and minimum temperatures of 27.6 °C and 15.2 °C, respectively.



Figure 3: Map of study area

### **1.11. Significance of the study**

Promoting universal access to electricity services is a key component of the Federal Government's commitment to reduce poverty. At present, for small and remote communities, micro-hydro power can be the best energy solution. As compact fluorescent light technology has become cheaper and more affordable for villages, a smaller amount of power generated can go a lot further in terms of lightning more households. Generally, for electric power generation to the rural areas which are detached from the main grid line, the following advantages can be realized.

**The quantifiable benefits:** Lighting and operation of radios, Fans and televisions, Essential health services and the development of economic opportunities, especially in agriculture and micro enterprises.

**Non-quantifiable benefits:** However, its effects on socio-political and employment creation for the people including rural population is also high.

### **1.12. Study methodology**

The overall study methodology adopted for this research work includes Analytical Studies and Computational fluid dynamics modeling will be carried out using ANSYS Fluent V18.0. Generally, to accomplish the above objectives of the research, the following logical diagram as shown below.



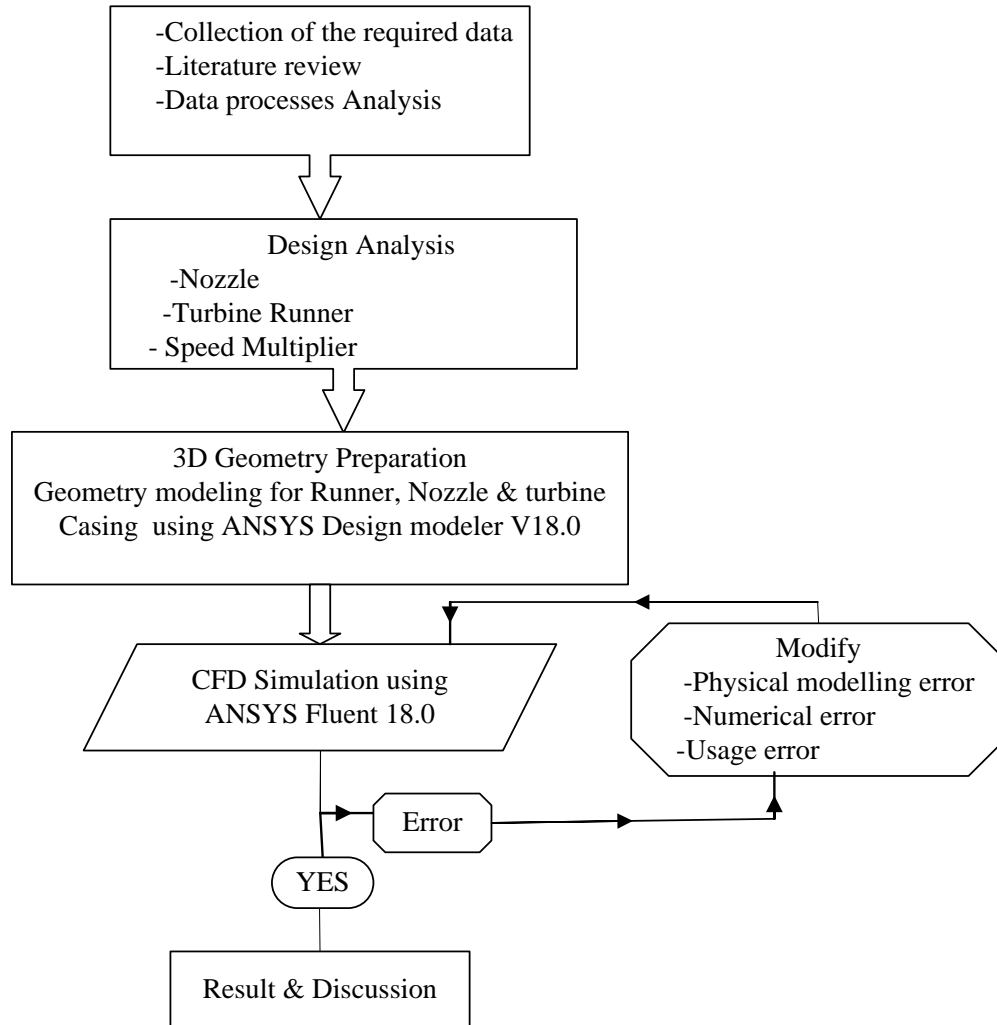


Figure 4: Flow chart of the study design

### 1.13. Structure of the Thesis

This section provides an outline of the thesis and briefly describes the contents of the following chapters.

**Chapter 1-** Deals with General Background, Hydro-power Classification by Size, Importance of micro hydropower, Description of Cross Flow Turbine, Problem the Statement, Objectives, Research Methods, Significance of the Study, Scope and Limitations of the Study and Organization of the study are discussed.

**Chapter 2 - Literature Review:** provides an overview of literature published and establishes the state of the art in the field of interest.

**Chapter 3-** Design of cross flow turbine components & speed multiplier: Deals with site data, Design profile of nozzle, calculating potential power and efficiency, Theoretical design of cross flow turbine runner, Design blade angle and blade velocity of turbine runner, Theoretical torque and force transfer in the turbine stages, Percentages of power that produced from both stages and design of speed multiplying mechanism.

**Chapter 4-** CFD Analysis of cross flow turbine: Introduction to Computational Fluid Dynamics, Application of CFD Analysis in Hydraulic Turbine Design, Limitations of The CFD Methodology, Governing Equations and Their Discretization, Numerical Grid Generation, Pre-processing and Convergence Criteria, Post-Processing the Results, Torque and efficiency, CFD Analysis Technique, Geometry Modeling and computational mesh generation, Solver Setup, Boundary Conditions, Selection of the physical models, Convergence Criteria and Solution Initialization.

**Chapter V-** Computational Results and Discussions: Graphical Display of (Pressure Distribution on the cross flow turbine, Velocity vectors and streamlines), and Efficiency Comparison.

**Chapter VII-** Conclusions and Recommendations: presents the outcomes of the research, reflects on the goals set. Moreover, this chapter provides a list of recommendations for future work.

## **CHAPTER 2. LITERATURE REVIEW**

This chapter provides an overview of the published relevant literatures to establish state of the art in the field of interest. Many researchers have studied the flow and performance characteristics of cross flow turbines experimentally, theoretically and using CFD tools. Some of the studies/researches are reviewed here as follows.

### **2.1. General Description of Hydropower**

Hydropower is one of the renewable energy source that comes from the kinetic or potential energy stored in water. Thus, fast moving water is a source of hydrokinetic energy that can be

tapped for electricity production or some other useful purpose. In addition, water stored high above a lower location is a source of hydro potential energy. The ultimate source of hydropower is solar energy. The sun evaporates water from the sea or other body of water and the wind drives the moisture overland. The moisture turns into a cloud after condensation and eventually falls to the earth's surface as rain or snow. Gravity attracts water from a high to low altitude and this flowing water is used to produce an energy form useful to humankind [9].

The primary prerequisite for the hydropower plant development is the availability of the potential resource in the proposed site. As a site specific energy resource, there are few factors that need to be considered in the technical development of a hydropower plant. First of all, the characteristic of the project will rely on the site's topography [10]. The next characteristic is related to the hydrology and the hydraulics, which is the volume of water discharge rate and the available head. The water discharge rate is defined as the volume of water that flows in unit of time ( $m^3/s$ ), while the head is defined as the difference between two water levels, measured in meter. Subsequently, once the topography, hydrology, and hydraulic data are collected and verified, it will be accounted as the base of plant design.

## **2.2. Hydropower classification by type**

Hydropower plants are often classified in three main categories according to operation and type of flow. Storage (reservoir), pumped storage hydro power plants (HPPs) and Run-of-river all vary from the very small to the very large scale, depending on the hydrology and topography of the watershed.

### **2.2.1. Storage Hydropower (Conventional Plant)**

The most common type of hydroelectric power plant is an impoundment facility. An impoundment facility, typically a large hydropower system, uses a dam to store river water in a reservoir. Water released from the reservoir flows through one or more turbines, spinning it, which in turn activates a generator to produce electricity. The reservoir acts much like a battery, storing power in the form of water when demands are low and producing maximum power during daily and seasonal peak periods. This kind of plants will involve a major works in civil engineering, while also need to consider the geological configurations on the site. The main benefit of the reservoir construction is that it can retain months of water discharge in it. In addition, the dam construction can also adapt to the environment and social needs in the region, by providing additional benefit such as flood control and irrigation resources. However, the

status of reservoir hydropower plant as the renewable energy source is still debated. The general scheme of this hydropower plant is described in Figure 5.

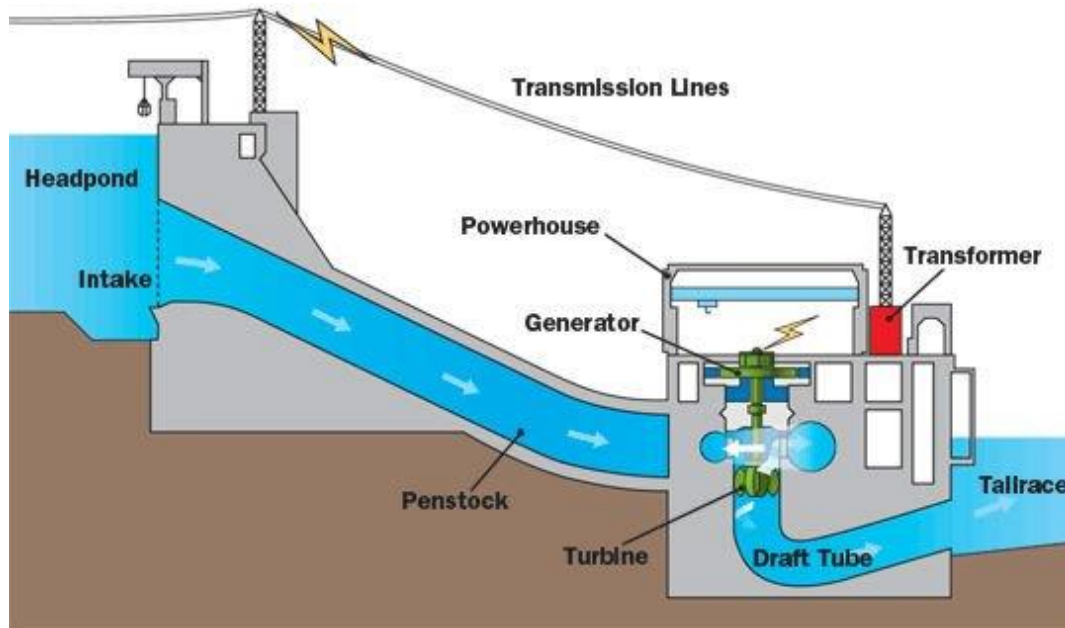


Figure 5: General Scheme of Reservoir Hydropower Plant [10]

There are many concerns and criticisms on the large reservoir hydropower plant that lead to harmful environmental effects, such as wildlife deterioration [10].

### 2.2.2. Pumped Storage plant (PSP)

Pumped Storage plant (PSP) is a type of hydropower plant that is used specifically for energy storage. This type of plant is the most widely applied energy storage technology. In 2009, about 100 GW of pumped storage plant was installed worldwide [11]. In PSP, there are at least two reservoirs, which is the upper reservoir and the lower reservoir. Water is pumped to upper reservoir to store energy when there is excess energy. The stored water in upper reservoir (Figure 6) then can be released to lower reservoir to move turbine, thus providing energy.

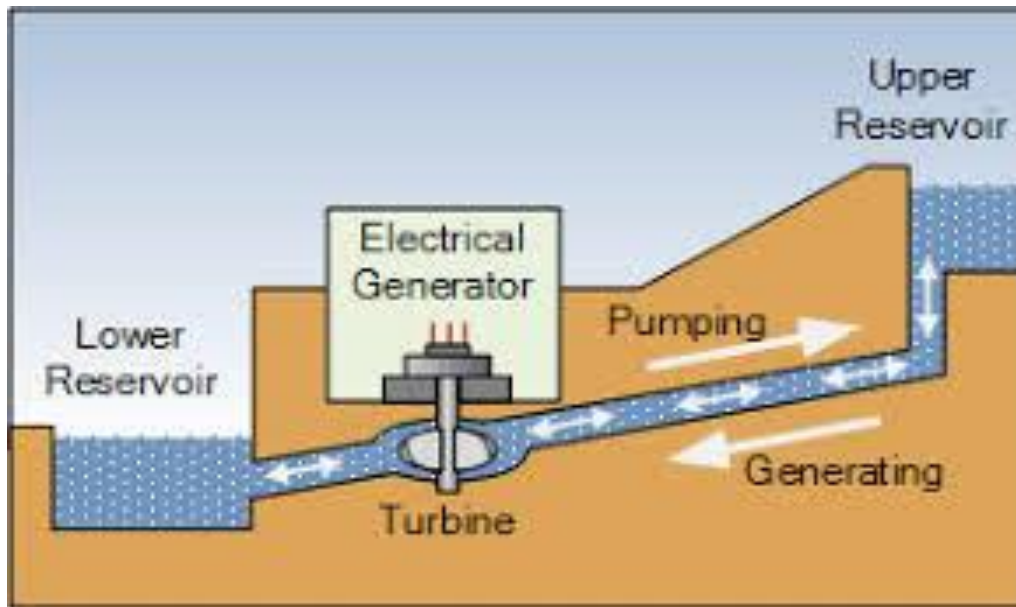


Figure 6: General Scheme of Pumped Storage Hydropower Plant [12]

The main limitation of this type of plant is that it relies heavily on topographic features, and only economically available on limited system characteristics. An advantage of pumped storage is that hydroelectric generating units are able to start up quickly and make rapid adjustments in output. They operate efficiently when used for one hour or several hours. Moreover, because pumped storage reservoirs are relatively small, construction costs are generally low compared with conventional hydropower facilities [12].

### 2.2.3. Run-of-the-River hydropower plants

Run-of-the-river hydroelectric stations are those with small or no reservoir capacity, so that only the water coming from upstream is available for generation at that moment, and any oversupply must pass unused. A constant supply of water from a lake or existing reservoir upstream is a significant advantage in choosing sites for run-of-the-river. Therefore, the energy available from this type of hydro power will heavily depend on the natural river flow conditions. It is a common scheme applied to mini or micro hydropower plants. The general scheme of this hydropower plant is described in Figure 7.

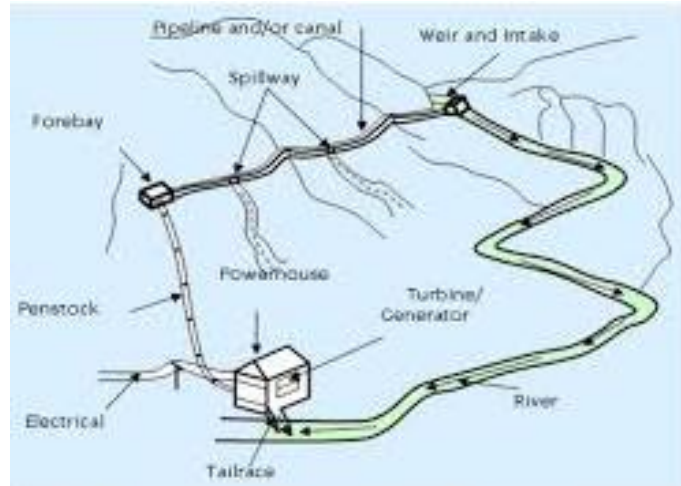


Figure 7: General Scheme of Run of River Hydropower Plant [13]

### 2.3. Types of Water Turbines

The turbine is the heart of hydropower system, where water power is converted into rotational force that drives the generator [14]. There are many types, sizes, and shapes of turbines that are used in hydropower systems, but in general, there are two categories of turbines: impulse turbines and reaction turbines. Depending on the head and the water discharge on the site, the selection of the turbine type is site specific. On Figure 8, it is shown that the application of different turbines on different sites is based on head and flow rate. A high head turbine, such as Pelton, has a lower specific speed.

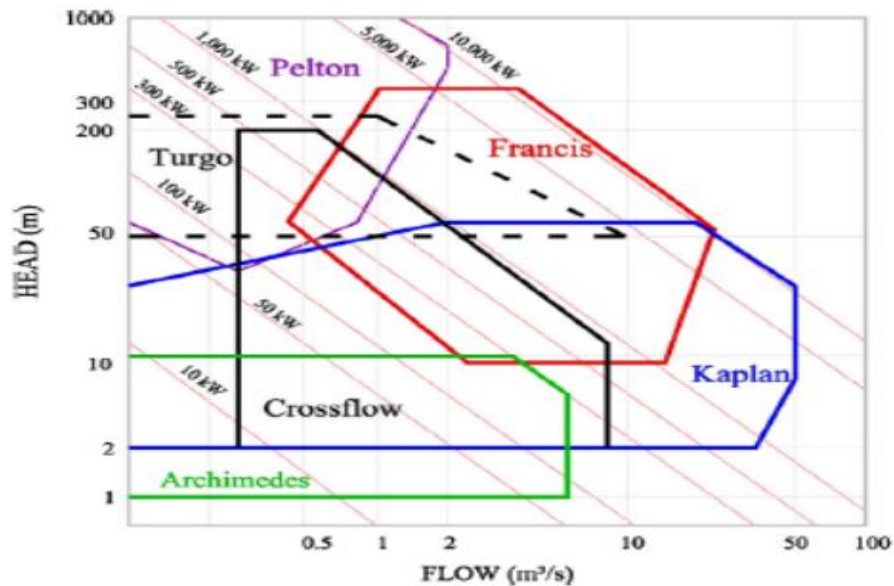


Figure 8: Different Turbine Application based on Head and Flow Rate [15].

The low-to-medium head turbine, such as Francis, has a medium specific speed. Similarly, a low head turbine, such as Propeller or axial flow turbine, has a very high specific speed and can handle very high flow rates. Crossflow turbine falls under low-to-medium head turbine with high specific speed. Use of these turbines in low-head systems requires the design of scaled versions, which tend to have lower efficiency than the full-scale versions. In addition, they are highly complex to design and manufacture locally and are also relatively expensive. Similarly, Turgo turbines, which require heads of about 50 m, is not as efficient as Pelton and Francis turbines, and has efficiency below 90%. Moreover, their blade design and manufacturing is also complex [15]. Therefore, improving the maximum efficiency would make crossflow turbines an ideal choice for small-scale applications. The typical efficiencies of those turbines are shown in Figure 9. In the selection of turbines for small-scale hydropower systems, the maximum efficiency, the simplicity in design and manufacturing, and the cost are tightly coupled. As shown in Figure 8, the crossflow turbine is the most suitable turbine for low-to-medium head of small systems. The simplicity in design and manufacturing at low cost is the most prominent feature amongst its counterparts. However, as shown in Figure 9, its maximum efficiency tends to be in the range 70 - 86%, which is lower than that of more commonly used advanced turbines, such as Pelton, Francis, and Kaplan, which have typical maximum efficiencies above 90% [16-17]. It is also known that compared to other turbines, crossflow turbines have relatively flat efficiency curves over a wide range of operating conditions as shown in Figure 9.

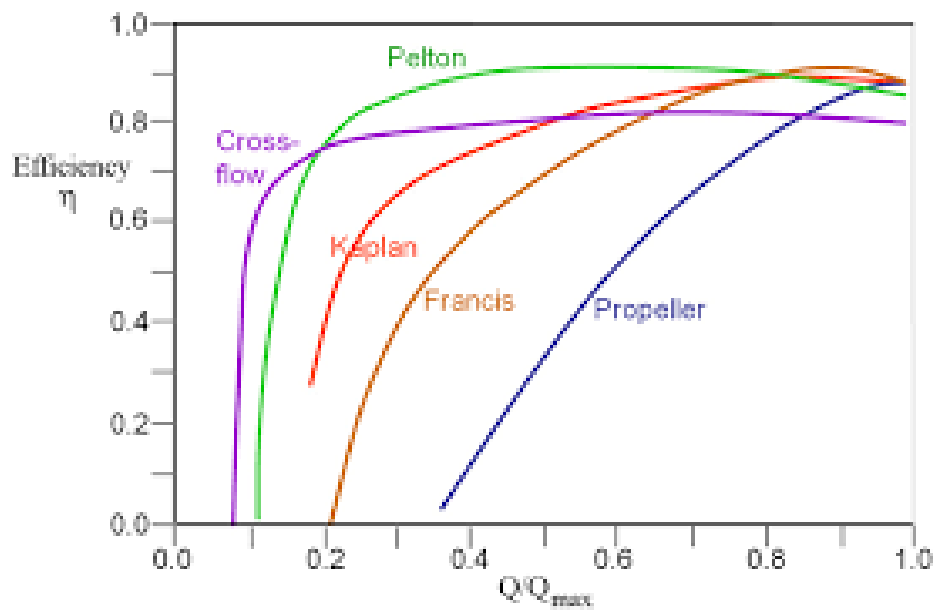


Figure 9: Comparison of typical efficiencies of different turbines [16].

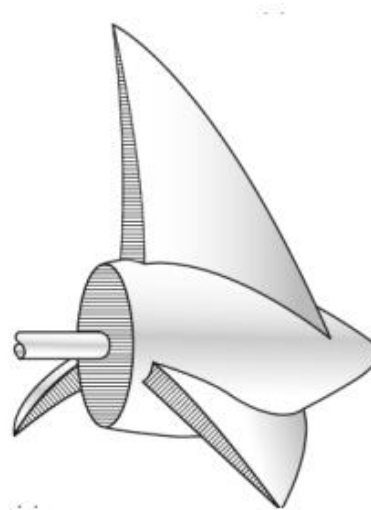
The most efficient impulse turbine, the Pelton wheel, normally operates above 50 m, whereas the reaction turbines like Francis and Kaplan can operate at low heads, but usually require high flow rates to operate at high efficiency.

#### 2.4. Reaction Turbine

Degree of reaction is the relative amount of pressure drop in the rotor and the nozzle, and is defined as the ratio of static pressure drop in the rotor to the static pressure drop in the stator or nozzle plus the rotor. In general reaction turbines produce power by combining the kinetic energy of the moving water and the potential energy available from the pressure difference. Popular examples of reaction turbines are Kaplan, Francis or Archimedes Screw. Usually reaction turbines are used for lower head (below 450m); reaction turbine is the standard choice [17]; higher flow applications than impulse turbines, and completely submerged in the water.



A. Francis Turbine



B. Propeller Turbine

Figure 10: Reaction Turbines [17]

The Francis turbine is used primarily for medium heads and large flow applications. They are an inward-flow reaction turbine that combines radial and axial flow concepts. This turbine was developed by James B. Francis in Lowell, Massachusetts in the 1800s. In the Francis turbine, the water discharges radially in the spiral casing, from the guide vane to the runner and exits axially (Figure 10(A)). This redirection of the flow causes the turbine to move. The blades in Francis turbine are fixed, so to regulate the flow, guide vane is used. In its operation, the runner is expected to have a high rotational speed, in order to achieve low torques at the axis, thus smaller



turbine size. The propeller and Kaplan turbines are advantageous for low head applications and thus enable sites that are previously cannot be harnessed by Francis turbine. Propeller turbine is used when the flow and head remain relatively constant [18]. Kaplan turbines have adjustable runner blades, thus providing better efficiency to the different flow rates. On the other hand, propeller turbines (Figure 10(B)) have fixed blades, which are not able to provide flexibility at changing flows, but provides high efficiency at design discharge.

## 2.5. Impulse Turbine

Impulse turbines, such as Pelton, work on the principle of impulse action of high jet velocity impinging on the impeller blades. All the available energy of the flow is converted into kinetic energy by the nozzle at atmospheric pressure before the flow passes through the turbine blades. Angular momentum is extracted by the blades mainly due to the dynamic pressure difference between the two surfaces of the blade, while the static pressure difference across the blade surface is atmospheric. Thus the impulse turbines have zero reaction. In contrast to this, the reaction turbines, such as Francis, Kaplan and Propeller, work on the principle of reaction forces developed across the blade surfaces. Angular momentum is extracted mainly due to the pressure drop across both the stationary guide vanes and the impeller blades. The pressure drop occurs both in the nozzle and the rotor. The Pelton turbine consists of series of cups that are attached around its wheel. To move the turbine, the jets of water directed to the series of cups, thus providing a tangential force to the turbine. The number of jets can be varied from one to multiple jets [19].

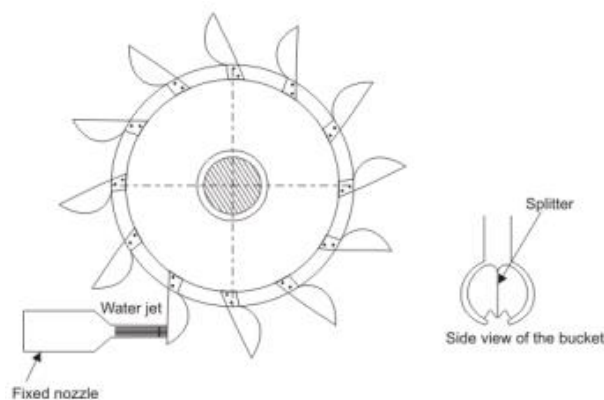


Figure 11: Pelton Turbine Side View with Fixed Nozzle [20]

As shown in side view of the bucket in the Figure 11, the cups consist of split bucket which split the jets in half. The jets then deflected at atmospheric pressure by the split buckets, turned back almost  $180^\circ$  in the process. To control the strength of the water jets, the flow of water through the

nozzle is controlled by a spear valve built in the nozzle. Another type of impulse turbine, turgo (Figure 12), is designed for the medium head applications (50-250m) [19]. Compared to a Pelton turbine, turgo turbine have different shape of buckets, while also having water jets at  $20^\circ$  angle. In this type of turbine, the water jets hit one side of the runner disk, and comes out on the other part of the runner.

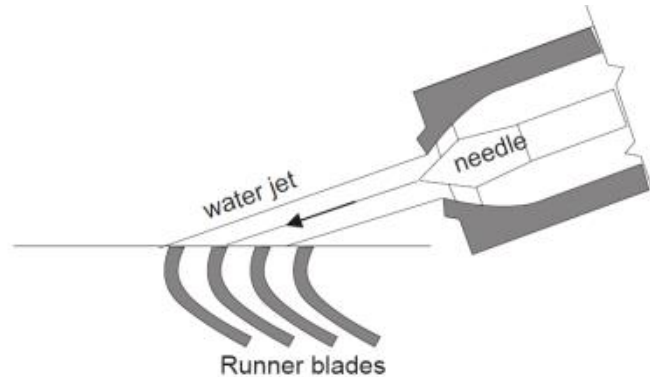


Figure 12: Water jet impingement on the turgo runner [22]

The Cross-Flow type (Figure 13), on the other hand, this is designed for lower heads compared to the other impulse turbine such as Pelton and turgo, this type of turbine provides lower efficiencies, but it can utilize larger water discharges [23]. The water discharges come through a rectangular shaped nozzle output, directed to a cylindrical runner by one or more guide vanes. The pressure remains constant in case of impulse turbine such as cross flow turbine at runner, whereas water enters tangentially in turbine runner at mid-way on one side. The flow of water crosses the turbine runner and moves in opposite direction of center then exits. Water is striking over blades on both sides of runner, and the total power produces by the turbines contributed 75% from the first stage and remaining part of power by second stage [24].

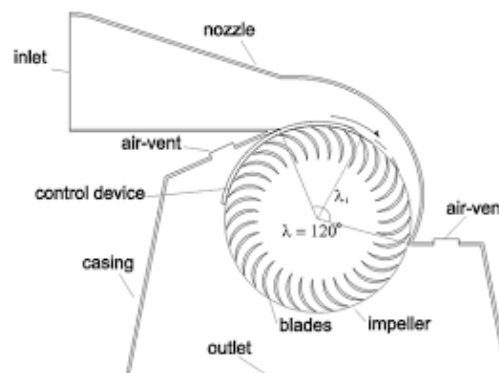


Figure 13: Cross Flow Turbine [24]

## 2.6. Review of previous studies related with the study topic

Hydropower on a small scale or micro-hydropower is one of the most cost-effective energy technologies to be considered for rural electrification in less developed countries [25]. Micro Hydropower (from hydro meaning water and micro meaning small scale) refers to electrical energy that comes from the force of moving water used to power a household or small village [26, 27]. The best geographical areas for MHP systems are those where there are steep rivers, streams, creeks or springs flowing year-round, such as in hilly areas with high year-round rainfall [28].

Small hydropower plants, on the other hand, is considered as the options that give minimal or even no impact to the environments. Since its capacity is usually less than 10 MW (although there are no internationally accepted definition, this type of plant is mainly designed as a run of river plants. Small hydropower plants require a small dam or a weir. In general cases, very minimum or no water is stored in the plants [29].

Micro-hydro generators are low speed machines of salient pole type, having a large number of poles, a large diameter and a short rotor. The mechanical energy in the form of rotation is transferred to the generator using a shaft. The generator then produces electric energy that will be transmitted to the grid. The basic parameters to be considered in the selection of a suitable type of electrical generator are Type of desired output, Hydraulic turbine operation modes and Type of electrical load, i.e. interconnection with the national grid, storage in batteries or an isolated system supplying variety of household or industrial loads [30].

Therefore, synchronous generator is used in most MHP systems because it has the ability to establish its own operating voltage and maintain frequency while it is operating in a remote location.

Table 4: Selection of Generator Type [31]

Size of scheme	Up to 10 Kw	10 to 15Kw	More than 15Kw
Generator	Synchronous/Induction	Synchronous/Induction	Synchronous
Phase	Single or Three Phase	Three Phase	Three Phase

Low head micro-hydropower stations present an attractive and efficient way for electricity generation in rural, remote and hilly areas because of the increment in the level of greenhouse gas emissions and fuel prices in these sites and they have become increasingly popular for

application at small rivers. MHP generation efficiency is generally in the range of 60–80%, Micro-turbines generate very reliable power though with very simple designs and fabrications [32-33]. Nevertheless, the selection of micro-hydropower turbines for achieving the most efficient and best result is rather difficult, as most turbines are designed for higher systems; they may be modified applicable for low head micro-systems, but the operational principle often does not change [33].

Chappell indicated that cross flow turbines manufactured out of standard Plexiglas plastic pipes or sheets can substantially reduce the cost of materials, manufacturing, and repairs. For micro-hydro power plants (less than 100kW in capacity), He claims that the savings on the capital costs are in the order of about 50% or US\$700/kw [34].

Adhau et al. carried out extensive study at two potential sites, and studied the hydrological data of one site for possible development of mini/micro-hydro-power plant. He concluded that irrigation projects are economically and technically viable for micro-power generation [35].

Khosrowpanah et al. investigated the effect of the number of blades, the runner diameter, and the nozzle entry arc under flow/head variations on the turbine performance and reported that the maximum efficiency of the CFT at any flow/head combination increases as the nozzle entry arc increases or the aspect ratio of the runner decreases and the efficiency obtained from the experimental and CFD analysis were found as 65% and 80% respectively [36].

Vincenzo et al. They are focused on theoretical frame work for a sequential design of the turbine parameters, taking full advantage of recently expanded computational capability. To this aim, they describe two steps procedure for banki-michel parameter design. In the first step, some criteria design parameters were theoretically estimated, on the basis of some simplifying assumptions. In the second step, the influence of efficiency of the remaining design parameters was analyzed by means of CFD numerical testing. And they apply these new design procedures for a specific power plant, for a give design point. In this test case the turbine with 35 blades and an attack angle equal to  $22^\circ$  exhibited at the design point a high efficiency equal to 86 % [37].

The experimental study of Aziz and Desai reveals that in only 2 out of 18 cases, an increase in the diameter ratio produced an increase in the predicted maximum efficiency under automatic

dynamometer speed control. They also concluded that somewhere in the vicinity of the diameter ratio of 0.68 the cross-flow is maximum and results in maximum efficiency due to second stage contribution. They also studied the effect of angle of attack on the turbine efficiency and concluded that the angle of attack should be around 24 degrees, an increase in the angle of attack from 24 to 32 degrees resulted in an increase in the predicted efficiency to 90% [38].

Nakase et al. conducted experiments to study the effect of nozzle shape on the performance of cross-flow turbines. The outer diameter of the runner was 315mm and the runner had 26 blades, with blade inlet and outlet angles of 30 and 90 degrees. By classifying the flow as going through two stages, they concluded that there are two types of flow in the cross-flow turbine. One is the crossed flow, which flows through two stages, and the other is uncrossed flow, which flows only through the first stage. The crossed flow constitutes a major portion of the flow which gives rise to flow contraction causing the flow to accelerate from the first stage to the second [39].

Olgun et al. studied the effect the runner and nozzle over the efficiency of cross flow turbine with variations in the ratio of runner diameter and gate opening for two dissimilar turbine nozzles operating under different heads investigated experimentally. The different performance parameters studied were power input, runaway speed, power output, reduced speed, and, turbine efficiency for different combinations of runner and nozzle. The results obtained from the study clearly indicated that the change in diameter ratios and heads brought about a negligible difference in the efficiency of the turbine. The highest efficiency obtained was 72% for the runner with a diameter ratio of 0.67 [40].

Eve Cathrin Walseth was conduct two different experiment to determine the flow pattern and torque transfer through the runner. A cross flow turbine manufactured by remote hydro light in Afghanistan was installed in The Waterpower Laboratory at The NTNU in September 2008 and efficiency measurement was performed on the turbine. A maximum efficiency of 78.6% was obtained at 5-meter head. The first experiment was to visualize the flow through the runner with use of the high speed camera. The second experiment measured the torque transfer to the runner by the use of strain gages. But the main objective was to determine the flow pattern and torque transfer through the runner [41].

Chiyembekezo S. Kaunda<sup>1</sup>, et al. Investigated, the flow profile in the turbine at best efficiency point and at operating conditions that are away from best efficiency point. Numerical method has also been used to calculate and predict the efficiency of the turbine. The flow physics in a Crossflow turbine runner is a two-phase with a movable free surface. Such flow physics is difficult to analyze even numerically. A procedure for numerical analysis was followed and ANSYS CFX was used to solve the governing equations and to process the simulation results. It has been observed that the numerically obtained flow profile compare favorably with the actual flow pictures. The hydraulic efficiency obtained with experimental turbine and numerical approaches were found as 78%, 82% respectively; which shows very good agreement between the two approaches [42].

Andrade et al. carried out simulations to analyze the pressure and velocity fields inside the cross flow turbine runner and also evaluated the performance of turbine with variation in the speeds. The absolute flow velocity angle was obtained for simulation at the runner entrance by using runner at one time and by eliminating it for the next iteration. And a sensitivity analysis was carried out to observe the change in flow angle along the nozzle and it was found in the analysis that the outlet angle was varying from 23° to 7° along the rotational angle. A good agreement was found between the experimental and numerical results, except in case of speeds more than 800 rpm then the result predicted by the numerical methods higher than the experimental result. The result shows that the energy transfers in first and second stage by the cross flow turbine are 68.5% and 31.5% respectively. Some fluid dynamic phenomenon was observed from the experiment like recirculation flow zones inside blade flow passage and shocks with runner shaft. For all the flow angles under study, downward peaks were found attributed to the location of runner blades [43].

Sammartano et al. describe a two-step design methodology for the optimal design of cross flow turbines but defined efficiency in terms of the head difference between inlet and outlet. This gives a higher value than the definition used here. The first step is a simple analytical nozzle design equation. The second gives a set of empirical values for the runner design, which can be refined using steady and unsteady RANS computations. A simulation of a 5.2 kW turbine of optimal design, using steady and unsteady RANS computations and the SST  $k-\omega$  turbulence

model and two-phase homogeneous model with free-surface effects, gave a maximum efficiency of 86%. However, this efficiency must be greater than the more common one used here [44].

### **2.7.Scientific Gap**

Review of different literaturesdictates further research works in the field of experimental and theoretical analysis of cross flow turbineneed to be conducted that could result in the development of a more efficient low head hydraulic turbine system that can provide an economical and efficient power generation system. among the system components to be studied are,

- ✓ Ultra-low head dual axis cross flow turbine that can minimiz shaft wear and bending due to weight of runner, and two twinturbines run with a nozzle and simple casingcould be investigated.
- ✓ To study the effect on the performance of ultra-low head cross flow turbine by increasing the rotational speed of runner.
- ✓ A simple speed multiplier with High efficiencies and reducing the overall sizes to achieve the required speed of the generator could be designed.

## CHAPTER 3. DESIGN OF CROSS FLOW TURBINE COMPONENTS

### 3.1. Site Data

The site is located in wonji-Shoa sugar factory irrigation canal flow with ahead of 2.85m and can thus be categorized as a low head and high flow rate site. The canal flow considering the dry season water flow, the volumetric flow rate available is  $1.02\text{m}^3/\text{sec}$  which is minimum during the dry season water flow.

### 3.2. Design Profile of Nozzle

The nozzle is the component with rectangular cross-sectional area, discharges the water which impinges on entire width of the turbine and usually enters the wheel at an angle of  $16^\circ$  with respect to tangential direction of the periphery of the rotating drum. The nozzle is designed with rectangular cross-section to minimize friction loss. Thus, loss due to friction in nozzle flow is reduced (minimized) due to its rectangular cross-section at the inlet and outlet[45]. Rectangular cross-section nozzle is used instead of circular cross-section.

#### 3.2.1. Bernoulli's Principle

From Bernoulli's Principle for a steady state the sum of all forms of energy along a streamline is the same at all points on that streamline. This requires that the sum of kinetic energy, potential energy and internal energy remains constant. Thus, an increase in the speed of the fluid, implying an increase in both its dynamic pressure and kinetic energy, occurs with a simultaneous decrease in its static pressure, potential energy and internal energy. There are three components in the formulation of the total head of a turbine. In equation 3.1, the subscript A indicate the inlet section of the nozzle; the subscript B indicate the outlet section of the nozzle.

- ✓ Pressure head is due to the static pressure, the internal molecular motion of a fluid that exerts a force on its container;
- ✓ Velocity head is due to the bulk motion of a fluid (kinetic energy);



- ✓ Elevation head is due to the fluid's weight, the gravitational force acting on a column of fluid;

In the Bernoulli equation (equation 3.1), Limitations on the use of the Bernoulli Equation the fluid should be [45].

- ✓ The fluid is an incompressible substance
- ✓ Flow through the nozzle is steady and one-dimensional flow
- ✓ Atmospheric pressure at both inlet and outlet condition.
- ✓ The fluid flow along a streamline
- ✓ The fluid ideally should not a viscosity (frictionless flow)

Now by applying Bernoulli equations between point A and B and from mechanical energy conservation the inlet velocity is gained.

$$\frac{P_A}{\rho g} + \frac{V_A^2}{2g} + Z_A = \frac{P_B}{\rho g} + \frac{V_B^2}{2g} + Z_B = Constant \quad 3.1$$

By assuming the fluid to be inviscid, the fluid motion is governed by pressure and gravity forces only. If the density and the specific weight are constant and the flow is steady along the streamlines, then the Bernoulli equation is valid. Thus, the total head at the inlet section (A) of the Nozzle is:

$$H_A = \frac{P_A}{\rho g} + \frac{V_A^2}{2g} + Z_A \quad 3.2$$

Meanwhile at the outlet section (B):

$$H_B = \frac{P_B}{\rho g} + \frac{V_B^2}{2g} + Z_B \quad 3.3$$

Where,  $\frac{P}{\rho g}$  represent the pressure head,  $\frac{V^2}{2g}$  is the velocity head and  $Z$  is the elevation head.

The total head or hydraulic head is defined as:

$$H_T = H_A - H_B \quad 3.4$$

Where,  $V_A = 0$  (at initial condition, the inlet velocity is small relative to the outlet) and ( $P_A = P_B = P_{atm}$ ) because water discharge in to the atmosphere.

Then, the Bernoulli equation simplifies to:

$$\frac{V_B^2}{2g} = Z_A - Z_B$$

$$V_B = \sqrt{2 \times g \times H_{net}} \quad 3.5$$

From this relation, it is clear the Bernoulli's principle: if there is not work supplied and the totalhead is constant. However, not all the hydraulic head can be convert into energy for there are always losses.

**Calculation of the Head Loss(m):** This includes the different losses of water flowing from the for bay tank until it penetrates the turbine runner, which include trash rack loss, entrance loss, fanning friction loss in the penstock, joint and bending losses, valve losses, and summing up all this results or considering 6-10% of the gross head [46].

**The head loss is defined as:**

$$H_{Losses} = H_{gross} \times 6\% \quad 3.6$$

$$H_{Losses} = 0.06 \times 2.85 = 0.171 \text{ m}$$

Therefore, it is possible now to define the Net Head:

$$H_{net} = H_{gross} - H_{Losses} \quad 3.7$$

which is equal to the total elevation head difference ( $Z_A - Z_B$ )

$$\text{Hence, } H_{net} = 2.68 \text{ meter}$$

Then, the discharge velocity of water in to the nozzle is given by equation 3.5,

$$V_B = \sqrt{2 \times g \times H_{net}}, \text{ where: } g = 9.81 \text{ m/sec}$$

$$V_B = \sqrt{2 \times 9.81 \times 2.68} = 7.25 \text{ m/sec}$$

The governing equations for fluid flow is analyzed by means of conservation laws: conservation of mass, conservation of momentum and conservation of energy. The law of mass conservation, which also is known as the continuity equation states that the rate of increase of mass inside an element is equal to the net flow rate of mass into the element across its faces.

The integral equation for the conservation of mass:

$$\int_{\partial V} \frac{\partial \rho}{\partial t} \partial \vartheta + \int_S \rho (V \times n) ds = 0 \quad 3.8$$

Where, the first integral corresponds to the control volume and the second one corresponds to the boundary surface of the control volume.

For the steady state case, the first term is eliminated. In case of incompressible flow, where the density variation is small and can be neglected and if the steady state one-dimensional flow assumptions are valid, the above equation can be written as:

$$Q = V_{in} A_{in} = V_{out} A_{out} \quad 3.9$$

Where:  $V$  and  $A$  are the velocity and the cross section area, respectively; and  $Q$  is the volumetric flow rate. Therefore, the continuity equation ( $Q = AV$ ) is used to express the volume flow rate  $Q$  as product of cross section area  $A$  and mean velocity  $V$ .

Then, the water inlet area of the nozzle can be determined from equation (3.9) as:

$$A_{in} = \frac{Q}{V_{in}} = \frac{1.02}{7.25} = 0.14 \text{ m}^2$$

The nozzle depth can be calculated as:

$$B_1 = B_2 + l \sin \alpha \quad 3.10$$

Where: the nozzle attack angle for maximum efficiency ( $\alpha = 16^\circ$ ), since maximum efficiency attain at this angle [46]. The length of the nozzle ( $l = 150\text{mm}$ ), the gap between the runners ( $= 60\text{mm}$ ) and the outlet of the nozzle depth ( $B_2 = 160\text{mm}$ ) are assumed values that depend on the nozzle geometries in order to minimize the loss in the nozzle fluid flow.

Therefore, the Nozzle depth is ( $B_1 = 243\text{mm}$ )

The height of nozzle inlet can be calculated by applying the continuity equation at the inlet section of the nozzle as:

$$Q = V_1 A_1 \quad 3.11$$

Where:  $A_1 = h_1 \times B_1$  is the inlet area of the nozzle,

$$\text{Hence, } h_1 = \frac{A_1}{B_1} = \frac{0.14 \text{ m}^2}{0.243 \text{ m}} = 0.576 \text{ m}$$

The outlet height of the nozzle ( $h_2$ ) is determined to be:

$$h_2 = h_1 - 2l \times \tan(16)$$

$$h_2 = 578 - 86 = 490\text{mm},$$

The outlet height of the nozzle is equal to the length of the runners to full utilization of water jet on the blade and the mass flow rate into a control volume must also be equal to the mass flow rate out of the control volume.

When the flow is uniformly distributed over the opening in the control surface (one dimensional flow), then the mass flow rate of water in the nozzle is:

$$\dot{m} = \rho AV = 1000 (0.14 \text{ m}^2 \times 7.25)$$

$$1.015 \frac{\text{kg}}{\text{sec}}$$

And the outlet area of the nozzle can be calculated as:

$$A_2 = B_2 \times h_2 = 0.16 \times 0.49$$

$A_2 = 0.0784m^2$  , which is equal to the area of water jet.

Here, the continuity equation may now be used again in order to express the results obtained only in terms of the two areas and the inlet mean velocity. Since the volume flow rate between the two sections is constant, the outlet velocity of flow from the nozzle is given by:

$$V_2 = \frac{m}{A_2} = \frac{1.015kg/sec}{0.0784m^2} = 12.94m/sec$$

$V_2 = 12.94 m/sec$ , It is clear that velocity increase from position 1 to 2, and pressure decrease.

The fluid velocity ratio between the section 1 and 2 can be calculated:

$$\frac{V_2}{V_1} = \frac{13}{7.25} = 1.79 \text{ (or an increase of 79\%)}$$

Therefore, the water velocity is increased by 79% as it flows through the rectangular nozzle.

### 3.2.2. The Linear Momentum

The governing equation for momentum is based on Newton's second law which relates the fluid particle acceleration to the sum of forces acting on a fluid particle and given as:

$$\sum \vec{F} = \vec{M} = \rho Q \vec{V} \quad 3.12$$

$$\sum F = \frac{\partial}{\partial t} \int_{cv} V \rho \partial \vartheta + \sum V_{out} \rho_{out} A_{out} - \sum V_{in} \rho_{in} A_{in}$$

Applying the momentum equation between the sections 1 and 2, Net outflow of momentum can be calculated as:

$$\sum F = \sum V_{out} A_{out} - \sum V_{in} A_{in} \quad 3.13$$

The entire mass flow rate of the nozzle at the control volume is constant and applying the momentum equation between the sections 1 and 2, then net outflow of momentum:

$$\begin{aligned} \text{Total mass within the CV: } m_{cv} &= \rho Q (\vec{V}_2 - \vec{V}_1) \\ &= 1000 \times 1.02(13 - 7.25) = 5.865 \text{KN} \end{aligned}$$

Since, the one dimensional fluid flow involves only horizontal momentum and there is no momentum accumulation because the structure is stationary, neglecting the momentum changes in the nozzle.

$$\sum F = \sum V_{out} A_{out} - \sum V_{in} A_{in} \quad 3.14$$

$$F_p - F_N = 0$$

Where:  $F_p$  is the force of pressure distribution to the inside of the nozzle and  $F_N$  is the external force acting on the nozzle.

Then, the force of pressure in the x- direction can be calculated as:

$F_P = P_{atm} \times A_1$ , where:  $P_{atm}$  is atmospheric pressure

$$F_P = \frac{101.325 \text{ kN}}{\text{m}^2} \times 0.14 \text{ m}^2 = 14 \text{ kN}$$

The resultant force is calculated as follows:

$$\begin{aligned} F_R &= F_P + F_N \\ &= 14 \text{ kN} + 8.135 \text{ kN} = 22.135 \text{ kN} \end{aligned}$$

### 3.2.3. Flow Controlling Mechanism

The pulsating and high load flow water is controlled by opening and closing the guide vane as the required position. This guide vane is a mechanical type which is driven by crank handle through its thread. It can move up to 80mm to cover the entire surface of each runner. Each turbine has its own guide vane. As a result, one turbine can operate when the other is fail or if there is no enough water capacity.

### 3.3. Determination of Potential Power and Efficiency of Cross Flow Turbine

The potential power that can be generated from the small hydro power plant is often calculated from the survey of the site. With net head and flow measurements, one can estimate the power output of the stream. The goal of the hydro power is to convert the available water energy into mechanical or electrical energy. The hydraulic power or hydro potential available from a river is directly related to the water flow rate and available head as given by equation (3.15).

#### 3.3.1. Hydraulic Power Input due to Head:

*Power input = Mass flow rate of water × Availabe Head*

$$P_{in} = \rho g Q H \quad 3.15$$

Where:  $\rho$  is the density of water ( $\text{kg}/\text{m}^3$ );  $g$  is the acceleration due to gravity ( $\text{m}/\text{s}^2$ );  $H$  is the effective pressure head of water across the turbine (m);  $Q$  is flow rate that is quantity of water flowing into turbine ( $\text{m}^3/\text{s}$ ).

The turbine power output is directly proportional to river flow and the elevation head (elevation difference between intake and exit) of the water falls. Theoretically, a river with twice the amount of flowing water should produce twice much energy. But in reality, there is friction of nozzle which decreases the output power. However, there will be some loss of power while the available water energy is converted by the hydropower plant.

Then, the magnitude of the absolute velocity at the exit of the nozzle (which is coincident with the turbine runner inlet) is given by:

$$V_1 = C_v^2 \sqrt{2gH_{net}} \quad 3.16$$

Where:  $V_1$  is the velocity that would exist at nozzle exit if losses were negligible;  $C_v^2$  is a coefficient smaller than unity, that accounts for the losses occurring inside the nozzle, together with any eventual departures of the flow from the assumption of one-dimensional flow[47].

Now, in this situation, solving for the power input and substituting the net head available in equation (3.17),

$$P_{in} = \dot{m} \times \left( \frac{V_B^2}{2C_v^2} \right) \quad 3.17$$

where,  $\dot{m}$  is the mass flow rate of water;  $P_{in}$  is the power input.

### 3.3.2. The Velocity Triangle of Cross Flow Turbine

An imaginary observer sitting on the blade of a revolving runner would observe flow through the runner as if looking at a stationary rectangular closed conduit. In contrast to flow through a stationary conduit, flow in the observed runner has the relative velocity in respect to the runner blade. However, a stationary observer outside the runner observes the absolute velocity of the moving fluid. The two velocities described are different by the peripheral velocity of the runner, with absolute velocity taking the higher value.

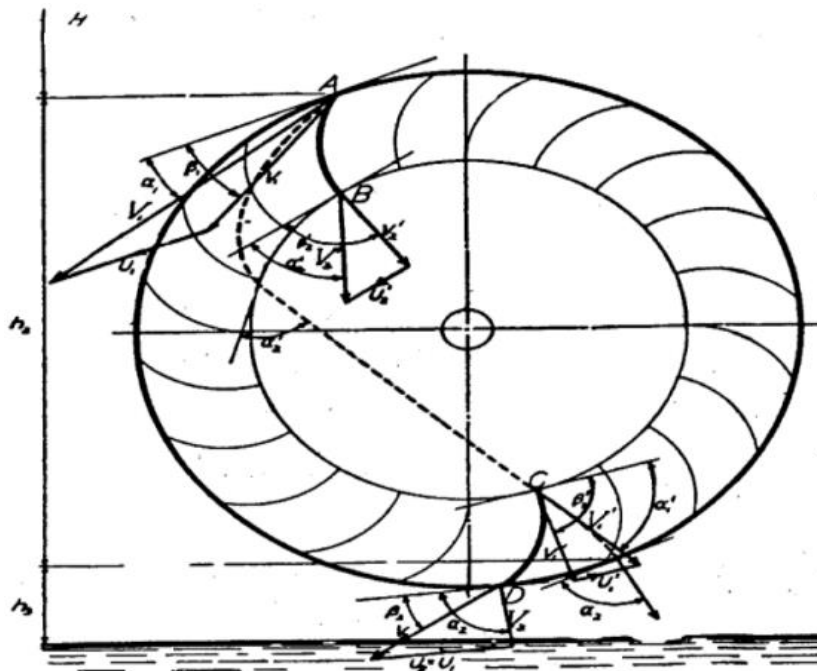


Figure 14: Theoretical velocity triangles of a cross- flow turbine runner

In order to calculate the force acting on the blade in the direction of motion,

$$F_x = \text{Mass flow rate of the fluid striking the blade} \times \text{Change of the Velocity of Whirl}$$

$$F_x = \dot{m} \times \Delta\omega \quad 3.18$$

Where:  $F_x$  is the force acting on the runner blade;  $\Delta\omega$  is the component of absolute velocity in the direction of blade inlet and outlet.

$$F_x = \dot{m}(V_{\omega 2} - V_{\omega 1}) \quad 3.19$$

Where:  $V_{\omega 1} = V_1 \cos \alpha_1$ ;  $V_{\omega 2} = -V_2 \cos \alpha_2$ .

The velocity triangles at inlet to the rotor, shown in Figure 14.

$V_{\omega 1}$  &  $V_{\omega 2}$  are in terms of attack angle and substituting in to equation(3.19),

$$F_x = \dot{m}(V_1 \cos \alpha_1 + V_2 \cos \alpha_2)$$

The force acting on to the blade in terms of blade inlet and exit angle, from velocity triangle,

$$V_{\omega 1} = V_{r1} \cos \beta_1 \text{ and } V_{\omega 2} = V_{r2} \cos \beta_2$$

$$F_x = \dot{m}(V_{r1} \cos \beta_1 + V_{r2} \cos \beta_2) \quad 3.20$$

$$F_x = \dot{m}V_{r1} \cos \beta_1 \left[1 + \frac{V_{r2} \cos \beta_2}{V_{r1} \cos \beta_1}\right] \quad 3.21$$

In order to take losses that occur inside the turbine runner into account, the relative velocity factor, ( $\psi$ ), is given by;

$$\psi = \frac{V_{r2}}{V_{r1}} \quad 3.22$$

where:  $\psi$  is a coefficient smaller than unity, that accounts for the losses occurring inside the runner, during the overall passage through the turbine runner, from point A to point B.

$$F_x = \dot{m}(V_1 \cos \alpha_1 - U_1) \left[1 + \frac{\psi \cos \beta_2}{\cos \beta_1}\right] \quad 3.23$$

### 3.3.3. Theoretical Power Output:

The theoretical power output from a site depends on the flow of the water and the height of the water fall at the site. In order to estimate the hydropower potential from a site, it is important that the head available from the canals and the flow of water over a period of time be measured. Power available is proportional to the product of head of water and discharge through the turbine.

The general formula for any hydro system's power output is as given in equation (3.24):

$$P_{out} = \rho g Q H \eta \quad 3.24$$

Where:  $\eta$  is the hydraulic efficiency of the turbine;  $P_{out}$  is the mechanical power produced at the turbine shaft (Watts).

Now, net work done per second on blade is given by,

$$P_{out} = \text{Force} \times \text{Velocity of blade} \quad 3.25$$

Then, the velocity of blade at the inlet radius is equal to the exit radius ( $U_1 = U_2$ ) [48], and this value in equation (3.25), the following expression is obtained:

$$P_{out} = \dot{m}(V_1 \cos \alpha_1 - U_1) \times \left[1 + \frac{\psi \cos \beta_2}{\cos \beta_1}\right] \times U_1 \quad 3.26$$

Where:  $\beta_1$  and  $\beta_2$  are the blade angle inlet and outlet, respectively.

Dividing equation (3.26) by the absolute velocity of water at the exit of the nozzle ( $V_1$ ) gives the following equation for power output:

$$P_{out} = \dot{m}(\rho \cos \alpha_1 - \rho^2) \times \left(1 + \frac{\psi \cos \beta_2}{\cos \beta_1}\right) \quad 3.27$$

Where:  $\rho$  is the blade jet velocity ratio which indicating the rotor blade geometries and it is a coefficient smaller than unity and which is given by [48].

$$\text{and } \rho = \frac{U}{V_1}$$

### 3.3.4. Calculating Theoretical Efficiency of Ultra-Low Head Cross Flow Turbine:

The efficiency is defined as ratio of the mechanical energy delivered by the rotor of the cross-flow turbine to the available hydro energy supplied to cross-flow turbine. The general formula for efficiency is given as in equation (3.28),

$$\eta = \frac{P_{out}}{P_{in}} \quad 3.28$$

$$\eta = \frac{2C_v^2 \times ((\rho \cos \alpha_1 - \rho^2) \times [1 + \frac{\psi \cos \beta_2}{\cos \beta_1}])}{V_1^2} \quad 3.29$$

In the above equation (3.29), putting ( $\beta_1 = \beta_2$ ), differentiating with respect to  $\frac{U}{V_1}$ , and then equating to zero gives the maximum efficiency as:

$$\eta_{max} = \frac{2C_v^2 \times (\rho \cos \alpha_1 - \rho^2) \times [1 + \psi]}{V_1^2} \quad 3.30$$

$$\eta_{max} = \frac{\partial \eta}{\partial \rho} = 0$$

$$\frac{\partial \eta}{\partial \rho} = \frac{2C_v^2 \times (\rho \cos \alpha_1 - \rho^2) \times [1 + \psi]}{V_1^2} = 0$$

$$= 2C_v^2 \times (\rho \cos \alpha_1 - 2\rho) \times [1 + \psi] = 0$$



$$= \cos \alpha_1 - 2\rho = 0$$

The blade jet velocity ratio,

$$\rho = \frac{U}{V_1} = \frac{\cos \alpha_1}{2}$$

Now, substituting the blade jet velocity ratio value in to equation (3.29) and the maximum efficiency ( $\eta_{\max}$ ) is

$$\eta_{\max} = C_v^2 \times \frac{\cos^2 \alpha_1}{2} (1 + \psi) \quad 3.31$$

The maximum turbine efficiency of cross flow turbine mainly depends on the angle of attack ( $\alpha = 16^\circ$ ) between the particle velocity and the tangential direction at the impeller inlet, the blade roughness coefficient ( $\psi = 0.98$ ) and Nozzle roughness coefficient ( $C_v = 0.98 - 0.95$ ) [46]. Then,

$$\eta_{\max} = 0.98^2 \times \frac{\cos^2(16)}{2} [1 + 0.98]$$

$$\eta_{\max} = 0.878 = 87.9\%$$

Therefore, the maximum efficiency turbine would be 87.9 percent.

The determination of the mechanical power that is extracted from the two turbines is:

$$P_t = 1000 \text{ kg/m}^3 \times 9.81 \text{ m/sec}^2 \times 1.02 \text{ m}^3/\text{sec} \times 0.878$$

$$P_t = 23544.98 \text{ watts} = 23.6 \text{ kw}$$

Hence, the power extracted form a single turbine is  $P_t = 11.8 \text{ Kw}$

### 3.4. Theoretical Design of Cross Flow Turbine Runner

Characteristics of Cross Flow Turbines [49] are presented as it follows.

- ✓ Cross flow turbine running at speeds calculated by the head they are operating (between 300 to 1500rpm).
- ✓ The turbine uses the head about 2-6 meters at minimum power (1-10kW) but up to 100 meters' head can besuitable for higher powers up to 500 kW.
- ✓ Cross flow runners have a definite operating 'range' transitionally between Propeller and Pelton turbine types.

#### 3.4.1. Calculating Rotational Speed of Turbine:

It is defined as the speed in(rpm) at which a turbine of homologous design would operate, if the runner were to reduce to a size which would develop one metric horse power under one-meter head. It is given by the following relation:

The correlation between specific speed ( $N_s$ ) and net head available from the canal or (River) is given by:

$$N_s = \frac{513.25}{H^{0.505}} \quad 3.32$$

Where:  $N_s$  is the specific speed of turbine in revolutions per minute (*r.p.m.*);  $H$  is the head in meter.

The specific speed of crossflow turbine in terms of the turbine power output, turbine speed in (*r.p.m.*) and net head is expressed in equation (3.33) as

$$N_s = \frac{N\sqrt{P_t}}{H^{0.745}} \quad 3.33$$

Where:  $N$  is rated speed of turbine in revolutions per minute;  $P_t$  is turbine output in kW.

Substituting this value in equation (3.32), the turbine speed is given by

$$N = \frac{513.25H_{net}^{(0.745-0.505)}}{\sqrt{P_t}}$$

$$N = \frac{513.25 \times 2.68^{0.745}}{\sqrt{11.8}} = 374.42 \cong 375 \text{rpm}$$

### The Runner Outer Diameter ( $D_o$ ) Determination:

At maximum turbine efficiency, the tangential velocity of runner outer periphery is given by equation (3.34).

$$V_1 = \frac{1}{2} C_v \sqrt{2gH_{net}} \times \cos \alpha \quad 3.34$$

Where:  $V_1$  is absolute velocity (m/s); angle of Attack is ( $\alpha = 16$ ) degree;  $C_v$  is the coefficient of velocity dependent upon the nozzle;  $H$  head at the point.

The following formula relates the runner rpm and runner tangential velocity as:

$$V_1 = \frac{\omega D_o}{2} \quad 3.35$$

$$V_1 = \frac{2\pi N D_o}{120}$$

Where:  $D_o$  is the turbine outer diameters in meter.

Substituting equation (3.35) in to equation (3.34), and the outer diameter of the runner is given by

$$\frac{1}{2} C_v \sqrt{2gH_{net}} \times \cos \alpha = \frac{2\pi N D_o}{120}$$

$$D_o = \frac{42.3 \times \cos \alpha_1 \times C_v \sqrt{H_{net}}}{N}$$

$$D_o = \frac{42.3 \times \cos 16 \times 0.98 \sqrt{2.68}}{375} = 0.21m \cong 0.3m$$

Since cross flow turbines are available in a number of rotor diameters, the calculated diameter is normally in 210mm steps from 100 to 500mm. The smaller diameter is for higher head sites, for low head site (from 2.5 to 5 meters), 300mm diameters are normally used [47]. Therefore, the nearest standard diameter for 2.68m head, the outside diameter of cross flow turbine is 300mm.

#### Runner Inner Diameter( $D_{in}$ ):

The runner with diameter ratio 0.67 is more efficient than the runners with diameter ratios of 0.54, 0.58 and 0.75. Therefore, the inner to outer diameter ratio for a cross-flow hydraulic turbine is 0.67 for maximum efficiency and the inner runner diameter is given by:

$$\frac{D_{in}}{D_o} = 0.67 \quad 3.36$$

$$D_{in} = 201mm$$

#### Thickness of the Jet Water Entrance( $t_j$ ):

$$t_j = \frac{11.7 \sqrt{H_{net}}}{N} \quad 3.37$$

$$= \frac{11.7 \sqrt{2.68}}{375} = 51.07mm$$

#### The Blade Spacing( $t_b$ ):

$$t_b = \frac{kD_o}{\sin \beta_1} \quad 3.38$$

$$t_b = \frac{26.1}{\sin(30)} = 52.2mm$$

#### Radial Rim Width:

Neglecting the blade thickness, the thickness ( $s_1$ ) (Figure 14), of the jet entrance, measured at right angles to the relative velocity, is given in terms of the blade spacing ( $t_b$ ).

$$S_1 = t_b \sin B_1 \quad 3.39$$

$$S_1 = 52.2 \times \sin(30) = 26.1mm$$

#### Number of Blades( $n$ ):

Although the optimal number of blades can only be determined experimentally, following is the mathematical procedure presented in Banki technical paper:

$$n = \frac{\pi D_o}{t_b} \tag{3.40}$$

$$n = \frac{\pi \times 300}{52.2} = 18.05, \text{ which gives number of blades to be } 18.$$

**Runner Length (L):**

$$L = \frac{Q \times N}{50 H_{net}} \tag{3.41}$$

$$L = \frac{0.51 \times 375}{50 \times 2.68} = 1.02m$$

In order to get highest speed of turbine due to its inertia the length of the turbine is equal to the height of the nozzle[47]. Therefore, the length of turbine runner is, (L = 490mm)

The distance between water jet and the center of runner shaft (y<sub>1</sub>);

$$y_1 = 0.116 \times D_o \tag{3.42}$$

$$y_1 = 0.116 \times 300 = 34.8mm$$

In a similar manner the distance between the outer edge of the jet and the inner periphery(y<sub>2</sub>), can be determined.

$$y_2 = 0.05 \times D_o \tag{3.43}$$

$$y_2 = 0.05 \times 300 = 15mm$$

**The Radius of Blade Curvature(R<sub>c</sub>)Determination:**

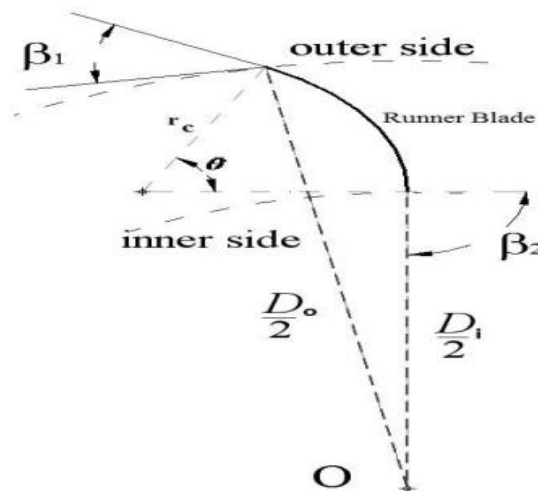


Figure 15: Runner blade profile

$$R_c = \frac{\frac{D_o}{4} [1 - (\frac{D_i}{D_o})^2]}{\cos \beta_1 + \frac{D_o}{D_{in}} \cos \beta_2} \tag{3.44}$$

$$R_c = \frac{\frac{300}{4} [1 - (\frac{201}{300})^2]}{\cos(30) + \frac{300}{201} \cos(90)} = 47.72mm$$

Therefore, the radius of blade curvature is  $R_c = 47.72 \text{ mm}$

**The Blade Curvature Angle Determination:**

The central angle ( $\theta$ ) of the blade angle, which depends basically on the inlet blade angle, is given by:

$$\frac{r_o}{r_i} = \frac{\sin(180 - \frac{1}{2}\theta)}{\sin[90 - (\frac{1}{2}\theta + \beta_1)]} \tag{3.45}$$

$$= \frac{\sin(\frac{1}{2}\theta)}{\sin(\frac{1}{2}\theta + \beta_1)}$$

$$\tan \frac{1}{2}\theta = \frac{\cos\beta_1}{\sin\beta_1 + \frac{r_i}{r_o}}$$

$$\tan \frac{1}{2}\theta = \frac{\cos(30)}{\sin(30) + \frac{100.5}{150}} = 0.740$$

$$\frac{1}{2}\theta = \tan^{-1}(0.740) = 36.5$$

Where:  $\theta$  is the blade central angle which comes out to be  $73.0^\circ$ . Using  $\beta_1 = 30^\circ$

**3.5. Design of Blade Angle and Blade Velocity of Cross Flow Turbine**

As shown in Figure(14), the velocity triangles at the exit of the first passage and inlet to the second passage are assumed to be equal, because there is no flow deflection in the rotor inside space and the pressure is constant there. Therefore, the contributions of these velocity triangles cancel exactly and are not further considered, traditionally, so that the only velocity triangles analyzed are those at inlet to the first passage and at the exit of the second passage. When the jet strikes the blades, two cases will be developed. The first helps to move the blade and the other one increases the range of flow velocity of blade. Therefore, from the velocity triangle shown in figure (14), the energy exchange takes place in the turbine runner. In this condition, the first stage blade inlet angle from the above velocity triangles is

$$U_1 = 0.5V_1 \cos \alpha_1, \text{ and} \tag{3.46}$$

Realizing that  $U_1 = U_2$  (the exit radius is equal to inlet radius),

$$\tan \alpha_1 = \frac{V_{r1} \sin \beta_1}{U_1 + U_2} = \frac{V_{r1} \sin \beta_1}{2U} \tag{3.47}$$

$$\tan \alpha_1 = \frac{V_{r1} \sin \beta_1}{2V_{r1} \cos \beta_1},$$

$$\tan \alpha_1 = 0.5 \tan \beta_1, \text{ putting the attack angle } \alpha_1 = 16^\circ$$

$$\tan \beta_1 = 0.573, \beta_1 = \tan^{-1}(0.573),$$

$$\beta_1 = 29.83^\circ \cong 30^\circ$$

First stage blade exit angle ( $\beta_2$ ) for a perfect radial flow should be equal to  $90^\circ$  and is equal to ( $\beta_1$ ) for maximum efficiency [45]. It is recommended to increase the blade exit angle above  $90^\circ$  in order to prevent shock losses. Thus, shock losses arise when the relative velocities of the first stage exit and second stage entrance are not concurrent.

#### Calculation of the Relative Velocity at the Inlet ( $V_{r1}$ ):

$$V_{r1} \cos \beta_1 = V_1 \cos \alpha_1 - U_1 \quad 3.48$$

Where:  $U_1$  is the first stage blade inlet velocity and it is given by

$$U_1 = 0.5V_1 \cos \alpha_1 = 0.5 \times 13 \cos 16 = U_1 = 6.25 \text{ m/sec}$$

$$V_{r1} = \frac{V_1 \cos \alpha_1 - U_1}{\cos \beta_1} = \frac{13 \cos 16 - 6.25}{\cos 30} = 7.23 \text{ m/sec},$$

#### Calculation of the Relative Velocity at the Exit ( $V_{r2}$ ):

In order to take losses that occur inside the rotor into account, it will be considered that [45].

$$V_{r2} = \psi V_{r1} \quad 3.49$$

Where:  $\psi$  is a coefficient that accounts for the losses occurring inside the rotor during the overall passage through the rotor from point (A) to point (B) and it is smaller than unity.

$$V_{r2} = \psi V_{r1} = 0.98 \times 7.23 = 7.085 \text{ m/sec}$$

The absolute Velocity of the first stage exit ( $V_2$ ), which is equal to that of second stage inlet,

$$V_2 = \sqrt{V_{r2}^2 + U_2^2} \quad 3.50$$

Where:  $U_2$  is blade exit velocity and it is given by

$$U_2 = V_{r2} \cos \beta_1 = 7.085 \times \cos 30 = 6.136 \text{ m/sec}$$

$$V_2 = \sqrt{7.085^2 + 6.25^2}$$

$$V_2 = V_3 = 9.448 \text{ m/sec}$$

#### Determination of the Whirl Velocity for First Stage at the Inlet and Exit:

The velocity vector which is responsible for producing torque in the tangential component also known as velocity of whirl will be determined as follows.

**For first stage:**

$$V_{\omega_1} = U_1 + V_{r_1} \cos \beta_1 \quad 3.51$$

$$V_{\omega_1} = 6.25 + 7.085 \cos 30 = 12.38 \text{m/sec}$$

$$\text{OR, } V_{\omega_1} = V_1 \cos \alpha_1 = 13 \times \cos 16 = 12.49 \text{m/sec}$$

**For second stage:**

$$V_{\omega_2} = V_{\omega_3} = U_2 \quad 3.52$$

$$= 7.085 \times \cos 30 = 6.136 \text{m/sec}$$

$$V_4 = V_{r_2} = 0.98 \times 7.23 = 7.085 \text{m/sec}$$

$$V_{\omega_4} = V_4 \cos \alpha_4,$$

It can be shown that, from the design for maximum efficiency, the flow must leave the second stage without whirl. Therefore,  $V_{\omega_4} = 0$

### 3.6. Theoretical Torque and Force Transferred in the Two Stages

Consider the flow through the runner passing through first stage as schematically shown in Figure 14 (inlet designated by (A) and outlet by (B)) and second stage (inlet designated by (C) and outlet by (D)). If Newton Second Law of motion is applied to a mass of water flowing with an infinitesimal velocity ( $d\vec{V}$ ) in a unit time in the direction of the velocity vector, then an infinitesimal force ( $d\vec{F} = \rho Q d\vec{V}$ ) is generated by the fluid. The infinitesimal reaction force ( $d\vec{F}_R$ ) on the blade is equal and opposite of the infinitesimal force, according to Newton Third Law of Motion. Therefore, the forces on the runner in the first stage ( $F_{1 \rightarrow 2}$ ) and second stage ( $F_{3 \rightarrow 4}$ ) are determined as follows:

**For the first stage:**

$$F_{1 \rightarrow 2} = - \int_1^2 \rho Q d\vec{V} = \rho Q (\vec{V}_1 - \vec{V}_2) \quad 3.53$$

$$F_{1 \rightarrow 2} = 1000 \times 0.51 (13 - 9.448) = 1811.52 \text{N} = 1.81152 \text{kN}$$

**For the second stage:**

$$F_{2 \rightarrow 3} = - \int_3^4 \rho Q d\vec{V} = \rho Q (\vec{V}_3 - \vec{V}_4) \quad 3.54$$

$$F_{2 \rightarrow 3} = 1000 \times 0.51 (9.448 - 7.085) = 1205.13 \text{N} = 1.20513 \text{kN}$$

The reaction to these forces provides the driving thrust on the runner ( $F_R$ ).

**The Reaction Force ( $F_R$ ):**

$$F_R = F_{1 \rightarrow 2} + F_{2 \rightarrow 3} \quad 3.55$$

$$F_R = 1.81152 + 1.20513$$

$$F_R = 3.01665kN$$

When using the equations (3.53) and (3.54), the absolute velocity vectors can also be expressed in terms of their orthogonal components, tangential component ( $V_\omega$ ) and radial components ( $V_F$ ). The velocity vector responsible for torque production is the tangential component, which is also known as velocity whirl. The radial component does not produce torque because its line of action passes through the axis of rotation. Therefore, taking multiplication of the force due to change in whirl velocity and its corresponding radius results in torque.

### 3.6.1. Percentages of Power Produced from Both Stages

#### Calculation of the Torque transferred on the first stage:

$$T_{1 \rightarrow 2} = \rho Q (\overline{V_{\omega 1}} \times R_1 - \overline{V_{\omega 2}} \times R_2) \quad 3.56$$

$$T_{1 \rightarrow 2} = 1000 \times 0.51 (12.38 \times 0.15 - 6.136 \times 0.1)$$

$$T_{1 \rightarrow 2} = 634.134 Nm$$

#### Calculation of the Torque transferred on the second stage:

$$T_{3 \rightarrow 4} = \rho Q (\overline{V_{\omega 3}} \times R_3 - \overline{V_{\omega 4}} \times R_4) \quad 3.57$$

$$T_{3 \rightarrow 4} = 1000 \times 0.51 (6.136 \times 0.1 - 0 \times 0.15)$$

$$T_{3 \rightarrow 4} = 312.936 Nm$$

#### The ratio of power transferred on both stages can be given as:

$$\frac{T_{1 \rightarrow 2}}{T_{3 \rightarrow 4}} = \frac{\rho Q (\overline{V_{\omega 1}} \times R_1 - \overline{V_{\omega 2}} \times R_2)}{\rho Q (\overline{V_{\omega 3}} \times R_3 - \overline{V_{\omega 4}} \times R_4)} \quad 3.58$$

Where: ( $U_1 = \omega R_1$ ), ( $U_2 = \omega R_2$ ), and for maximum Efficiency, the blade velocity is equal to the absolute velocity ( $U_1 = V_{r_1}$ ).

The Angular velocity of the runner ( $\omega$ ) is constant and from velocity triangles,

$$V_{\omega 1} = U_1 + V_{r_1} \cos \beta_1, U_1 + U_1 \cos \beta_1$$

$$V_{\omega 1} = U_1 (1 + \cos \beta_1),$$

$$V_{\omega 1} = \omega R_1 (1 + \cos \beta_1) \quad 3.59$$

Substituting terms of equation (3.59) in to equation (3.58),

$$\frac{T_{1 \rightarrow 2}}{T_{3 \rightarrow 4}} = \frac{\omega R_1 (1 + \cos \beta_1) R_1 - \omega R_2 \times R_2}{\omega R_2 \times R_2}$$

$$\frac{T_{1 \rightarrow 2}}{T_{3 \rightarrow 4}} = \left( \frac{R_1^2}{R_2^2} \right) \times (1 + \cos \beta_1) - 1$$



$$\frac{T_{1 \rightarrow 2}}{T_{3 \rightarrow 4}} = \left( \frac{0.15^2}{0.1^2} \right) \times (1 + \cos 30) - 1 = 3.198$$

$$\frac{T_{1 \rightarrow 2}}{T_{3 \rightarrow 4}} = 3.198$$

Therefore, the percentage contribution of each stage to total torque production is given by:

$$T_{1 \rightarrow 2} = 3.198 \times T_{3 \rightarrow 4} \quad 3.60$$

**The percentages of torque that are produced from first stage:**

$$\begin{aligned} \%T_{1 \rightarrow 2} &= \frac{T_{1 \rightarrow 2}}{T_{1 \rightarrow 2} + T_{3 \rightarrow 4}} \\ &= \frac{3.198 \times T_{3 \rightarrow 4}}{3.198 \times T_{3 \rightarrow 4} + T_{3 \rightarrow 4}} = 0.762 \end{aligned}$$

Similarly, for the second stage,

$$\begin{aligned} \%T_{3 \rightarrow 4} &= \frac{T_{3 \rightarrow 4}}{T_{1 \rightarrow 2} + T_{3 \rightarrow 4}} \\ &= \frac{T_{3 \rightarrow 4}}{3.198 \times T_{3 \rightarrow 4} + T_{3 \rightarrow 4}} = 0.238 \end{aligned}$$

They are found that about 76.2% of the power is produced at the first stage and the remaining at the second stage of the turbine, about 87.9% as maximum efficiency.

### 3.7.Design of Speed Multiplying Mechanism

Mechanical power transmission systems that multiply the angular speed under a constant transmission ratio represents the function of a large group of products known as speed multipliers. An increase in speed is needed because the turbines rotors turn at a much lower speed than is required by most electrical generators. The range in which the input angular speed must be increased. There are several options for coupling the generator to the turbine in hydro systems that allow an increase in speed (such as belts and gears). In this study, the output speed of the turbine is multiplied by designing one stage spur gear to the inlet speed of the generator. This gear is having straight teeth cut on the rim and parallel to the axis of rotation. It is most common and cost-effective type of gear that is designed to transmit motion and power between parallel shafts which rotate in the opposite direction. Since the compactness, cost of the design, ease of fabrication, and ease of maintenance are the most crucial element of design considerations for this work, the one stage spur gear is designed as the speed multiplier.

### 3.7.1. Basic Geometry of Spur Gears

The fundamentals of gearing are illustrated through the spur gear tooth as in Figure 17, both because it is the simplest and most comprehensible, and because it is the form most widely used, particularly for instruments and control systems. The basic geometry and nomenclature of a spur gear mesh is shown in Figure 17. The essential features of a gear mesh are:

1. Center distance and the pitch circle diameters (or pitch diameters).
2. Size of teeth (or module) and number of teeth.
3. Pressure angle of the contacting involutes.

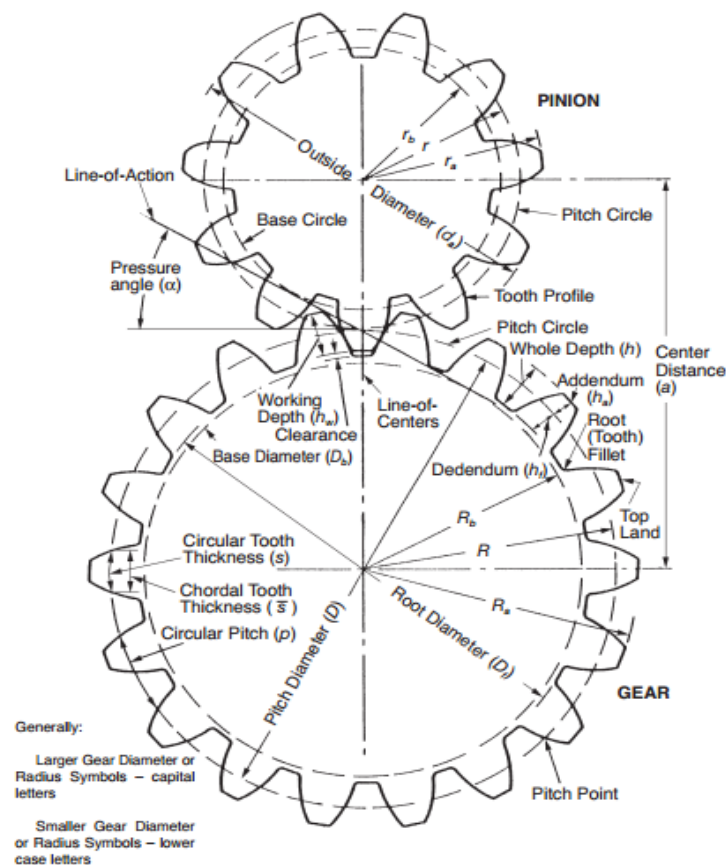


Figure 16: Basic Gear Geometry [50].

### 3.7.2. Design of One Stage Spur Gear Speed Multipliers

In the present analysis, the size of both pinion and larger gear, maximum torque, allowable stress and tangential load of the spur gear are calculated based on the designed power output and rotational speed of cross flow turbine. The desired generator specifications and the design assumptions of the required gear box design are as it follows.

- ✓ Two different types of materials are considered to design pinion and gear.

- ✓ Both gears in the gear box are spur gears.
- ✓ Thicknesses of the gears are same in a gear-pair.
- ✓ In a gear-pair, wheel is assigned the larger number of teeth between the mating gears.

A one stage spur gear box is required to transmit 11.8kW power from a turbine shaft rotating at 375rpm to a generator shaft rotating at 1500rpm. When designing a spur gear, there are many important factors to be considered such as weight, size, strength, durability, material and geometry of the gear.

### 3.7.2.1. Material Selection for the Gears

The first step in the gearbox design process is to select the material. A material is to be selected by doing intensive research on the properties of the various materials. The materials used for manufacturing of gears depend upon the strength and service conditions like wear, compactness with size, and noise. The gears maybe manufactured from metallic or non – metallic materials. In most cases, Alloy steel is widely used for manufacturing of gears due to its good wear resistance properties, excellent machinability and ease of producing complicated shapes by casting method and other parameters. For the sake of designing the gearbox, AS-4600 and AS -4140 are selected as pinion and gear materials, respectively, due to their better mechanical properties, especially for reducing weight.

Table 5: Material Specifications [51]

Elements	Material	Bending stress ( $\sigma_b$ )	Crushing Stress ( $\sigma_c$ )	Modulus of Elasticity (E)
Pinion	AS -4600	400N/mm <sup>2</sup>	1100N/mm <sup>2</sup>	$2.15 \times 10^5 N/mm^2$
Gear	AS -4140	320N/mm <sup>2</sup>	950N/mm <sup>2</sup>	$1.6 \times 10^5 N/mm^2$

### 3.7.2.2. Determination of Speed Ratios and Number of Teeth

Speed ratio is the ratio of the speed of driving gear to the speed of the driven gear and it is given as it follows.

#### Calculation of the Speed Ratio ( $i$ )

$$i = \frac{N_P}{N_G} = \frac{Z_G}{Z_P} \quad 3.61$$

Where:  $N_P$  and  $N_G$  = Angular velocity of driver and driven gears (rpm), respectively; and  $Z_P$  and  $Z_G$  = Number of teeth on driver and driven gears, respectively.

$$i = \frac{N_P}{N_G} = \frac{1500}{375} = 4$$

If the mating gear has more teeth than the pinion, that is speed ratio is more than one, then the smallest number of teeth on the pinion without interference is given by [52].

$$N_p = \frac{2k}{(1+2i)\sin^2\phi} \left( i + \sqrt{i^2 (1 + 2i)\sin^2\phi} \right) \quad 3.62$$

where:  $k = 1$  for full depth teeth and  $\phi = 20^\circ$ , which is pressure angle.

$$N_p = \frac{2 \times 1}{(1 + 2 \times 4)\sin^2(20)} \left( 4 + \sqrt{4^2 (1 + 2 \times 4)\sin^2(20)} \right)$$

$$= 15.35 \approx 16 \text{ teeth}$$

$$i = \frac{Z_G}{Z_P}, Z_G = Z_P \times 4 = 64 \text{ teeth}$$

Thus, a 16 teeth pinion will mesh with a 64 teeth gear without interference.

### 3.7.2.3. Calculation of Lewis Form Factor:

Spur gears are manufactured mostly with involute profile and pressure angles of  $14.5^\circ$  or  $20^\circ$ . However, the  $20^\circ$  pressure angle of gears are widely used because of their high load carrying capacity. Hence, the Lewis form factor for pinion is given by:

$$Y = \pi \left( 0.154 - \frac{0.912}{Z} \right) \text{ for pressure angle } (\phi = 20^\circ) \quad 3.63$$

Hence, the Lewis form factor for pinion ( $Y_P$ )

$$Y_P = \pi \left( 0.154 - \frac{0.912}{Z_P} \right), = \pi \left( 0.154 - \frac{0.912}{16} \right) = 0.3047$$

The Lewis form factor for pinion is 0.3047 for 16 teeth.

Similarly, Lewis form factor for Gear ( $Y_G$ )

$$Y_G = \pi \left( 0.154 - \frac{0.912}{Z_G} \right), = \pi \left( 0.154 - \frac{0.912}{64} \right) = 0.439$$

Therefore, the Lewis form factor for both largest and pinion gear were found as 0.439 and 0.3047, respectively.

### 3.7.2.4. Determination of Weaker Member:

For pinion ( $S_P$ );

$$S_P = \sigma_b \times Y_P \quad 3.64$$

$$400 \times 0.3047 = 122 \text{ N/mm}^2$$

For Gear ( $S_G$ );

$$S_G = \sigma_b \times Y_G$$

$$320 \times 0.439 = 140.48N/mm^2$$

Then, the minimum value of these stresses, which help to calculate the module value, will be selected for the weaker member. Therefore, the pinion is weaker member.

### 3.7.2.5. Estimation of Module based on Beam Strength

Two fundamental stress equations are used in the American gear manufacturing Association (AGMA) methodology, one for bending stress and another for pitting resistance (contact stress). Since both the gears are made of the different materials, the pinion is weaker than the gear. The minimum number of teeth for 20° pressure angle is 16 teeth.

Hence, the module (m) for spur gear is calculated by,

$$m = 1.26 \sqrt[3]{\frac{[M_T]}{Y_P \times \sigma_b \times \phi \times Z_P}} \quad 3.65$$

and the torque transmitted by pinion is calculated by using power equation,

$$P = \frac{2\pi N_P M_T}{60} \quad 3.66$$

$$\text{Where: } M_T = \frac{11.8 \times 10^3 \times 60}{2\pi \times 1500} = 75.121 Nm$$

And the initial design torque  $[M_T]$  can also be determined by,

$$[M_T] = M_T \times k_o \times k \times k_d \quad 3.67$$

Where: Shock factor ( $k_o = 1.5$ ); Load concentration factor ( $k = 1.02$ ); Dynamic load factor ( $k_d = 1.4$ ), and  $\phi =$  it is assumed that the ratio  $\left(\frac{b}{m}\right)$  is 10 [53].

$$[M_T] = 75.121 \times 1.5 \times 1.02 \times 1.4 = 160.909 Nm$$

$$m = 1.26 \sqrt[3]{\frac{[M_T]}{Y_P \times \sigma_b \times \phi \times Z_P}}, 1.26 \sqrt[3]{\frac{160.909 \times 1000}{0.3047 \times 320 \times 10 \times 16}} = 4.3 mm$$

Hence, module,  $m = 4.3 mm$ . On the basis of the above value, the module is selected to be 5mm according to the standard values of modules and this value of module has been verified as per the design result. Since the contact stresses of the gear are reduced by increasing the module of the gear, the next higher standard value of module is taken as 5mm.

### 3.7.2.6. Design of Both Larger Gear and Pinion Sizes:

The size determination of the gears starts with the calculation of module for spur gear. Once the module is determined, its value will be used to calculate other parameters of the gear such as

addendum, Dedendum, clearance, working depth, whole depth, clearance, outer diameter, and etc.

Table 6: Theoretical calculations of conventional Spur gear

No.	Item	Symbol	Formula	Pinion	Gear
1	Pitch circle diameter	D	$modul \times Number\ of\ teeth$	80	320
2	Circular Pitch	P	$\pi \times module$	15.7	
3	Addendum	$a$	Addendum = $module(m)$	5	
4	Dedendum	$d$	$1.25 \times module$	6.25	
5	Outside Diameter	$D_o$	$D + 2 \times module$	90	330
6	Root circle diameter	$D_R$	$pitch\ diameter - (2.5 \times m)$	67.5	307.5
7	Base circle diameter	$D_b$	$D \cos\phi$	75.2	300.7
8	Tooth Thickness	$T_t$	$(\pi \times module)/2$	6.3	
9	Base Pitch	$P_b$	$m\pi \cos\phi$	15	
10	Center distance	C	$\frac{D_G + D_P}{2}$	240	
11	Face width	$b$	$3\pi \times module$	50	
12	Bottom clearance	$C_b$	Addendum – Dedendum	1.25	
13	Tooth height	T	Addendum + Dedendum	11.25	

\* All linear dimensions in millimeters for Table 6

All calculated values in Table 6 are based on the determined module, m, and number of teeth of the pinion and gear.

### 3.8. Checking for Design of Pinion Gear:

#### 3.8.1. Design based on Contact Strength

The contact stress is given by

$$\sigma_c = 0.74 \left( \frac{i \pm 1}{C} \right) \sqrt{\frac{(i \pm 1) E [M_T]}{ib}} \quad 3.68$$

Where: (i+1) for external gearing and (i-1) for internal gearing

$$\sigma_c = 0.74 \times \left( \frac{4 + 1}{240} \right) \sqrt{\frac{(4 + 1) 2.15 \times 10^5 \times 160.909 \times 1000}{4 \times 50}} = 453.4 \text{ N/mm}^2$$

Hence, because  $453.4N/mm^2 < 1100N/mm^2$ , the design is safe.

### 3.8.2. Design for Pinionbased on Bending Stress

$$\sigma_b = \frac{(i+1)[M_T]}{c \times m \times b \times Y_p} \quad 3.69$$

$$\sigma_b = \frac{(4 + 1)160.909 \times 1000}{240 \times 5 \times 50 \times 0.3047} = 44N/mm^2$$

Since  $44N/mm^2 < 400N/mm^2$ , then the design is safe.

The torque transmitted by gear is determined as:

$$M_T = \frac{11.8 \times 10^3 \times 60}{2\pi \times 375} = 300.48Nm$$

and the design torque $[M_T]$  is determined as:

$$[M_T] = M_T \times k_o \times k \times k_d$$

Where: Shock factor ( $k_o = 1.5$ );( $k = 1$ )and ( $k_d = 1.4$ );(Assumed).

$$[M_T] = 300.48 \times 1.5 \times 1 \times 1.4 = 631.02Nm$$

### 3.8.3. Design for Pinion Based on Dynamic Load

The tooth surface strength of pinion $F_p$ (in kN) is calculated as:

$$F_p = [\sigma_b] \times Y_p m b \quad 3.70$$

$$F_p = 400 \times 0.3047 \times 5 \times 50 = 30470N = 30.47kN$$

The dynamic load on the pinion gear tooth is given by

$$F_{d_p} = 2 \frac{[M_t]}{d_p} \times \frac{5.5 + V_m^{1/2}}{5.5} \quad 3.71$$

and the Pitch Line Velocity,

$$V = \frac{\pi D_p N_p}{60} = \frac{\pi \times 0.08 \times 1500}{60} = 6.28m/sec$$

$$F_{d_p} = 2 \times \frac{16090}{80} \times \frac{5.5 + (6.3)^{\frac{1}{2}}}{5.5} = 5.85kN$$

For the design to be safe, the tooth surface strength ( $F_p$ ) must be greater than the dynamic load on gear tooth( $F_{d_p}$ ),  $F_p > F_{d_p}$ . Therefore, the design is safe for surface durability consideration.

### 3.9. Design Based on Wear strength

#### 3.9.1. Calculation of the Maximum Wear Load for Pinion

The maximum load the gear tooth is able to transmit power without pitting failure. This ability of the gear is known as the wear strength of the gear tooth. The load stress factor( $k$ ) defined in this theory is as it follows.

$$k(\text{Loadstressfactor}) = \frac{\delta_c^2 \sin(\phi) \times \left(\frac{1}{E_1} + \frac{1}{E_2}\right)}{1.4} \quad 3.72$$

Where:  $\sigma_c$  is the maximum compressive stress;  $\phi$  is the pressure angle;  $E_1$  and  $E_2$  are the modulus of elasticity of the materials of the two mating gears.

$$F_w = Q \times d_p \times b \times k \quad 3.73$$

Where:  $p$  subscript is for driving gear and  $g$  subscript is for driven gear.

Ratio factor ( $Q$ ) is defined in this theory as:

$$Q = \frac{2Z_g}{Z_g - Z_p} = \frac{2 \times 64}{64 - 16} = 2.67 \text{ for the case of maximum wear.}$$

$$k = \frac{(1082.06)^2 \sin(20) \times \left(\frac{1}{2.15 \times 10^5} + \frac{1}{1.6 \times 10^5}\right)}{1.4} = 3.12 \text{ N/mm}^2$$

$$F_w = 80 \times 2.67 \times 50 \times 3.12 = 33321.6 \text{ N}$$

For the design to be safe, the tooth wear load ( $F_w$ ) must be greater than the dynamic load on gear tooth ( $F_{dp}$ ),  $F_w > F_{dp}$ . Therefore, the design is safe for tooth wear load consideration.

### 3.10. Checking for Design of Larger Gear:

#### 3.10.1. Design for Gear Based on Induced Bending Stress

$$\sigma_b = \frac{(i+1)[M_T]}{c \times m \times b \times Y_g} \quad 3.74$$

$$\sigma_b = \frac{(4+1) \times 1000 \times 631.02}{240 \times 5 \times 50 \times 0.448} = 119.78 \text{ N/mm}^2$$

Hence,  $119.78 \text{ N/mm}^2$  is less than  $320 \text{ N/mm}^2$  and the design is safe.

#### 3.10.2. Design for Gear Based on Induced Contact Stress

$$\sigma_c = 0.74 \times \left(\frac{i+1}{c}\right) \sqrt{\frac{(i+1)E \times [M_T]}{i \times b}} \quad 3.75$$

$$\sigma_c = 0.74 \times \left(\frac{4+1}{240}\right) \sqrt{\frac{(4+1)1.6 \times 10^5 \times 1000 \times 631.02}{4 \times 50}} = 774.54 \text{ N/mm}^2$$

$774.54 \text{ N/mm}^2 < 950 \text{ N/mm}^2$ , hence the design is safe.



### 3.10.3. Design for Gear Based on Dynamic Load

Calculation of beam strength for Gear or the tooth surface strength of pinion is as it follows.

$$F_G = [\sigma_b] \times Y_G m b \quad 3.76$$

$$F_G = 320 \times 0.439 \times 5 \times 50 = 35120N = 35.12kN$$

The dynamic load on the largest gear tooth is given by

$$F_{d_g} = 2 \frac{[M_t]}{d_g} \times \frac{5.5 + V_m^{1/2}}{5.5} \quad 3.77$$

$$F_{d_g} = 2 \times \frac{631020}{320} \times \frac{5.5 + (6.3)^{1/2}}{5.5} = 5743.70N = 5.74kN$$

Therefore, since  $F_G > F_{d_g}$ , the design is safe for surface durability consideration.

### 3.10.4. Calculation of the Maximum Wear Load for Gear

$$k = \frac{(774.54)^2 \sin(20) \times \left( \frac{1}{2.15 \times 10^5} + \frac{1}{1.6 \times 10^5} \right)}{1.4}$$

$$k = 2.30N/mm^2$$

$$F_w = Q \times d_g \times b \times k \quad 3.78$$

$$F_w = 320 \times 2.67 \times 50 \times 2.30 = 98256N = 98.25kN$$

Hence,  $F_w > F_{d_g}$ ,  $98.25kN > 5.74kN$ , and the design is safe in wear load.

## **CHAPTER 4. COMPUTATIONAL FLUID DYNAMICS MODELING OF TURBINE**

In this chapter, the concept of computational fluid dynamics and the usage of this tool for the present work are explained. The required physics for solving the runner by this approach is also described. Moreover, this chapter includes verification of various assumptions introduced in the model to reduce the computational cost. Subsequently, this section provides the details of setting up a simulation in ANSYS Fluent and running the calculations.

### **4.1. Introduction to Computational Fluid Dynamics**

Computational Fluid Dynamics (CFD) is the analysis of systems involving fluid flow, heat transfer and associated phenomena such as chemical reactions by means of computer-based simulation. The heat and mass transfer, fluid flow, chemical reaction, and other related processes that occur in engineering equipment, in the natural environment, and in living organisms play a vital role in a great variety of practical situations. Nearly all methods of power production involve fluid flow and heat transfer as essential processes. The same processes govern the heating and air conditioning of buildings. Major segments of the chemical and metallurgical industries use components such as furnaces, heat exchangers, condensers, and reactors, where thermo-fluid processes are at work.

Computational fluid dynamics (CFD) probably plays a greater part in the aerodynamic design of turbomachinery than it does in any other engineering application. For many years, the design of a modern turbine or compressor has been unthinkable without the help of CFD and this dependence has increased as more of the flow becomes amenable to numerical prediction.

Nowadays, Computational Fluid Dynamics (CFD) is a widely used method for the analysis and the design of hydraulic turbines. The accuracy of computational fluid dynamics is rapidly increasing, thanks to the available computational resources that allow simulating high-speed flows using high-fidelity methodologies. Computers are used to perform the calculations required to simulate the interaction of liquids and gases with surfaces defined by boundary conditions. With high-speed supercomputers, better solutions can be achieved.

#### **4.2. Computational Fluid Dynamics Analysis in Hydraulic Turbine Design**

The application of numerical methods to turbomachinery dates back to the 1940s. In fact, methods were even formulated before the advent of the digital computers that were necessary to implement them. The fundamental basis of almost all computational fluid dynamics problems are the Navier–Stokes equations, which define any single phase (gas or liquid, but not both) fluid flow. The development of the high speed computer software and evaluation of CFD have a great influence on the engineering design and analysis of turbomachinery. As computers and their associated design software become tools of design, development time reduces appreciably. CFD improves the design techniques when used in making computational experiments to understand the flow physics and the following advantages associated with this advanced numerical methodology [54].

The modern computer visualization of flow fields helps the turbine designer understand the flow in turbine passage better. The intuitive representation of the flow fields makes the potential problems of the design easily identified. This can reduce the hydro dynamic losses and improve the performance of the turbine system.

The numerical rigs can reduce the turbine development time and costs and the numerical simulation is satisfactory and can replace the model experiment, which is costly and time consuming. The turbo machinery flows can be more accurately predicted. This allows designers to explore more design alternatives, which would otherwise be too much time consuming or are outside the range of previous experience.

The application of CFD in hydraulic design enables designers to have better control on the flow behavior. Higher turbine loading and flow capacity can be achieved without causing detrimental flow phenomena such as flow separation, cavitation and choking. In consequence, the size and, therefore, the cost of the turbine can be reduced.

### **4.3. Limitations of Computational Fluid Dynamics Methodology**

Every engineering design method has its limitations. It is important for the designers to be aware of these limitations and the sources of error and accuracy of the method. Otherwise, it could lead to wrong products when the design method is applied outside its applicability ranges. The sources of error associated with CFD flow analysis can be divided into two broad categories: modeling errors and numerical errors [55].

The modeling error category includes errors due to the assumptions and approximations in the mathematical representation of the physical process and errors due to the incorporation of the empirical data into the model.

The modeling errors is related to the mathematical equations, geometry, boundary conditions, and turbulence models. It is obvious that the simplification of mathematical equations and geometry of the computational domain and the deviation of boundary conditions from the actual flow pattern can cause system errors in the CFD simulation. Among all this sources, the most challenging one is the one that is related to turbulence models. None of the currently known turbulence models has universal validity.

The numerical errors are caused by the uncertainties in the empirical coefficients in the model such as the “Constants” for the turbulence model. This source of errors becomes less significant as more experimental data are taken with more advanced measuring methods and tools. The numerical errors include computer round-off errors and error due to the numerical schemes which includes the aspects such as discretization, grid density and orthogonally, artificial dissipation and convergence [55]. The most discussion worthwhile aspect is the grid density, i.e. the grid dependency of CFD simulations. It is obvious that the finer the grid, the better the prediction, the costs, and time of the simulation.

### **4.4. Governing Equations and their Discretization**

The use of computational flow dynamics is a numerical methodology for solving the governing equations of fluid flow. The governing equations of fluid flow are partial differential equations,

when discretized on a mesh, they will be transformed into algebraic equations which can be solved by a finite-difference/finite-volume algorithm. The following sections will briefly describe the governing equations, flow conditions and properties employed in this work.

#### 4.5. Governing Equations of Fluid Flow

Computational Fluid Dynamics is the art of replacing such Partial Differential Equations (PDE) system by a set of algebraic equations which can be solved using digital computers. Fluid (gas and liquid) flows are governed by partial differential equations which represent conservation laws for the mass, momentum, and energy in Cartesian coordinate systems and they can be written as it follows.

##### 4.5.1. Principle of Conservation of Mass:

$$\frac{\partial \rho}{\partial t} + \frac{\partial(\rho u)}{\partial x} + \frac{\partial(\rho v)}{\partial y} + \frac{\partial(\rho w)}{\partial z} = \frac{\partial p}{\partial t} + \nabla(\rho V) = 0 \quad 4.1$$

Where:  $V$  is the velocity of fluid (m/sec);  $p$  is the pressure (N/m<sup>2</sup>); and  $\rho$  is the density of fluid (kg/m<sup>3</sup>).

This equation is the general form of the mass conservation equation and valid for incompressible as well as compressible fluids.

##### 4.5.2. Principle of Conservation of Momentum

Choosing the  $y$ -coordinate to be in the vertical direction opposite to the direction in gravity, the buoyancy forces act in the  $y$ -direction. The conservation of momentum equations in the Cartesian coordinates can be written as:

$x$ -Momentum Equation:

$$\frac{\partial}{\partial t}(\rho u) + \frac{\partial}{\partial x}(\rho uu) + \frac{\partial}{\partial y}(\rho vu) + \frac{\partial}{\partial z}(\rho wu) = -\frac{\partial p}{\partial x} + \mu \left( \frac{\partial^2 u}{\partial x^2} + \frac{\partial^2 u}{\partial y^2} + \frac{\partial^2 u}{\partial z^2} \right) \quad 4.2$$

$y$ -Momentum Equation:

$$\begin{aligned} \frac{\partial}{\partial t}(\rho v) + \frac{\partial}{\partial x}(\rho uv) + \frac{\partial}{\partial y}(\rho vv) + \frac{\partial}{\partial z}(\rho wv) \\ = -\frac{\partial p}{\partial y} + \mu \left( \frac{\partial^2 v}{\partial x^2} + \frac{\partial^2 v}{\partial y^2} + \frac{\partial^2 v}{\partial z^2} \right) - \rho g \beta (\Delta T) \end{aligned} \quad 4.3$$

Where,  $\Delta T = T_{\infty} - T$

$z$ -Momentum Equation;

$$\frac{\partial}{\partial t}(\rho w) + \frac{\partial}{\partial x}(\rho uw) + \frac{\partial}{\partial y}(\rho vw) + \frac{\partial}{\partial z}(\rho ww) \quad 4.4$$

$$= -\frac{\partial p}{\partial z} + \mu \left( \frac{\partial^2 w}{\partial x^2} + \frac{\partial^2 w}{\partial y^2} + \frac{\partial^2 w}{\partial z^2} \right)$$

#### 4.5.3. Principle of Conservation of Energy:

The physical principles of energy conservation are the first law of thermodynamics. The energy equation is given below as:

$$\frac{\partial}{\partial t} (\rho c_p T) + \frac{\partial}{\partial x} (\rho u c_p T) + \frac{\partial}{\partial y} (\rho v c_p T) + \frac{\partial}{\partial z} (\rho c_p T) \quad 4.5$$

$$= k \left( \frac{\partial^2 T}{\partial x^2} + \frac{\partial^2 T}{\partial y^2} + \frac{\partial^2 T}{\partial z^2} \right) + s_m \quad 4.5.1$$

These equations along with the conservation of energy equation form a set of coupled nonlinear partial differential equations. It is not possible to solve these equations analytically for most engineering problems. However, it is possible to obtain approximate computer based solution to the governing equations for a variety of engineering problems. The numerical analysis of CFD in cross flow turbine consists of incompressible fluid flow that reduces equations to the conservation of mass and momentum only. In addition, the temperature effect is negligible during the analysis for the flow of an isothermal Newtonian fluid. Therefore, the conservation of energy is ignored during this analysis.

#### 4.6. Discretization Method

The second step is to approximate the differential equations by a system of algebraic equations for the variables at some set of discrete locations in space and time. The most important discretization methods are finite difference (FD), finite volume (FV) and finite element (FE) methods all of which yield the same solution if the computational domain is very fine.

##### 4.6.1. Finite Difference Method

Finite difference method (FDM) describes the unknown flow variables of the flow problem by means of point samples at node points of a grid coordinate. By FDM, the Taylor's expansion is usually used to generate finite differences approximation.

Advantages:

- ✓ Relatively easy implementation,
- ✓ Good results and efficiency on simple geometries, and
- ✓ Several high-order schemes are available.

Disadvantages:

- ✓ Generally limited to structured meshes,

- ✓ Conservation property is not guaranteed in general, and
- ✓ For non-uniform grids, a coordinate transformation to the “Computational space” has to be considered and discretized consistently (Jacobian of coordinate transformation, from the chain rule).

#### 4.6.2. Finite Element Method

Finite element method (FEM) uses the simple piecewise functions valid on elements to describe the local variations of unknown flow variables. Governing equation is precisely satisfied by the exact solution of flow variables.

Advantages:

- ✓ Integral formulation: valid for shocks and discontinuities,
- ✓ Flexible for Complex geometries, and
- ✓ Straightforward high-order and Very rigorous mathematical foundation.

Disadvantages:

- ✓ Higher Computational effort, Conservation not always guaranteed.

#### 4.6.3. Finite Volume Method

Finite Volume Method was originally developed as a special finite difference formulation. The CFD Solver FLUENT is a finite volume based code for the simulations and modeling of fluid flow as well as heat transfer. Basically, the numerical algorithm in these Computational Fluid Dynamics commercial packages involves the formal integration of the governing equation over all the finite control volume; the discretization process involves the substitution of a variety of Finite difference method types to approximate the integration equation of the flow problem, and the solution is obtained by iterative method. Discretization in the solver involves these approaches to solve the numerical integration of the flow problem. Usually, two different approaches are made, one at a time.

Advantages:

- ✓ Directly apply the integral spatial discretization in the physical space (no coordinate transformation to a computational space, unlike Finite Difference Method and typically Finite Element Method),
- ✓ Flexible for complex geometries: both structured and un-structured meshes, and
- ✓ Mass, momentum and energy are conserved by definition.

Disadvantages:

- ✓ Historically, less developed mathematical framework (i.e. compared to finite element method), and
- ✓ More difficult to attain high order accuracy (compared to finite difference and finite element method), specially for unstructured meshes.

#### **4.7. Numerical Grid Generation**

The discrete locations at which the variables are to be calculated are defined by the numerical grid which is essentially a discrete representation of the geometric domain on which the problem is to be solved. It divides the solution domain into a finite number of subdomains (elements, control volumes etc.). Most common options are as follows:

##### **4.7.1. Structured (regular) Grid**

This is the simplest grid structure, since it is logically equivalent to a Cartesian grid. Each point has four nearest neighbors in two dimension and six in three dimensions. The disadvantage of structured grids is that they can be used only for geometrically simple solution domains. Another disadvantage is that it may be difficult to control the distribution of the grid points: concentration of points in one region for reasons of accuracy produces unnecessarily small spacing in other parts of the solution domain and waste of resources.

##### **4.7.2. Unstructured Grid**

For very complex geometries, the most flexible type of grid is one that can fit arbitrary solution domain boundary. In principle, such grids are applicable to any discretization scheme; however, they are best adapted to the finite volume and finite element approaches. In practice, grids made of triangles or quadrilaterals in 2D, and tetrahedral or hexahedral in 3D are most often used.

#### **4.8. Pre-processing**

The pre-processor contains all the fluid flow inputs for a flow problem. It can be seen as a user-friendly interface and a conversion of all the input into the solver in CFD program. At this stage, quite a lot of activities are carried out before the problem is being solved. These stages are listed below:

- ✓ Geometry Definition - The region of interest that is the computational domain which has to be defined.
- ✓ Grid generation- It is the process of dividing the domain into a number of smaller and non-overlapping sub-domains.



- ✓ Physical and chemical properties - The flow behavior in terms of physical and chemical characteristics are to be selected.
- ✓ Fluid property Definition - The fluid properties like density and viscosity are to be defined.
- ✓ Boundary conditions - All the necessary boundary conditions have to be specified on the cell zones.

The boundaries (such as walls, inlets and outlets) are also defined in this step. The solution of the flow problem such as temperature, velocity, pressure etc. is defined at the nodes inside each cell.

#### 4.9. Convergence Criteria

The convergence criteria are pre-set conditions on the residuals which indicate that a certain level of convergence has been achieved. For example, a criterion that the scaled residual for the x-momentum drop to 0.001 indicates that the overall error in this variable is about three orders of magnitude less than the bulk x-momentum in the system. Finally, one needs to set the convergence criteria for the iterative method. When using iterative solvers, it is important to know when to quit. The most common procedure is based on the difference between two successive iterates or residuals; the procedure is stopped when this difference, measured by some norm, is less than a pre-selected value. Many iterative solvers require calculation of the residual. The norm of residual prior to the first iteration provides a reference for checking the convergence of iterations (usually by three or four orders of magnitude).

#### 4.10. Post-Processing of the Results

After the simulation was completed, post-processing of the results took place. The computational fluid dynamics package provided the data for visualization of the results of the flow problem. This includes vectors plots, domain geometry and grid display, line and shaded counter plots and particle tracking. Recent facilities are aided with animation to display dynamic results, and they also have data export facilities for further manipulation of external to the code.

#### 4.11. Torque and Efficiency

The torque on the rotating parts is defined as follows:

$$T = \left( \int_S (\bar{r} \times (\bar{\tau} \cdot \hat{n})) dS \right) \hat{a} \quad 4.6$$

Where:  $S$  is representing the surfaces comprising all rotating parts;  $r$  is the position vector;  $\tau$  is the total stress tensor;  $\hat{n}$  is a unit vector normal to the surface;  $\hat{a}$  is a unit vector parallel to the axis of rotation.

The hydraulic efficiency of the cross flow turbine is internally calculated by Fluent. The ratio can be expressed as:

$$\eta = \frac{T\omega}{Q(p_1 - p_2)} \quad 4.7$$

Where:  $T$  is the net torque acting on the runner (N-m);  $\omega$  is the angular speed (rad/sec);  $Q$  is discharge through turbine ( $\text{m}^3/\text{sec}$ );  $P_1$  is total pressure at the inlet of the nozzle;  $p_2$  is the total pressure at the exit of the runner.

#### 4.12. Computational Fluid Dynamics Simulation Methodology

The methodology of this study is adopted in four steps. The first step is the generation of the three dimensional geometry as per the standard design; the second step is meshing the geometry; third step provides the boundary conditions as per data available at the site; the last step is simulating the model and observe the results in the post processor. After determining the important features of the particular problem of ultra-low head cross flow turbine were determined, the following basic procedural steps were taken.

##### 4.12.1. Geometrical Modeling

The runner and nozzle are the main parts of a cross flow turbine. The 3D geometry of both the rotating fluid domain and stationary fluid domain of dual axis cross flow turbine was modeled by using ANSYS Design Modeler Workbench 18.0 such as runners, nozzle, shaft, and turbine casing. Subsequently, the designed 3D geometry of the dual axis cross flow turbine is shown in the figure (17).

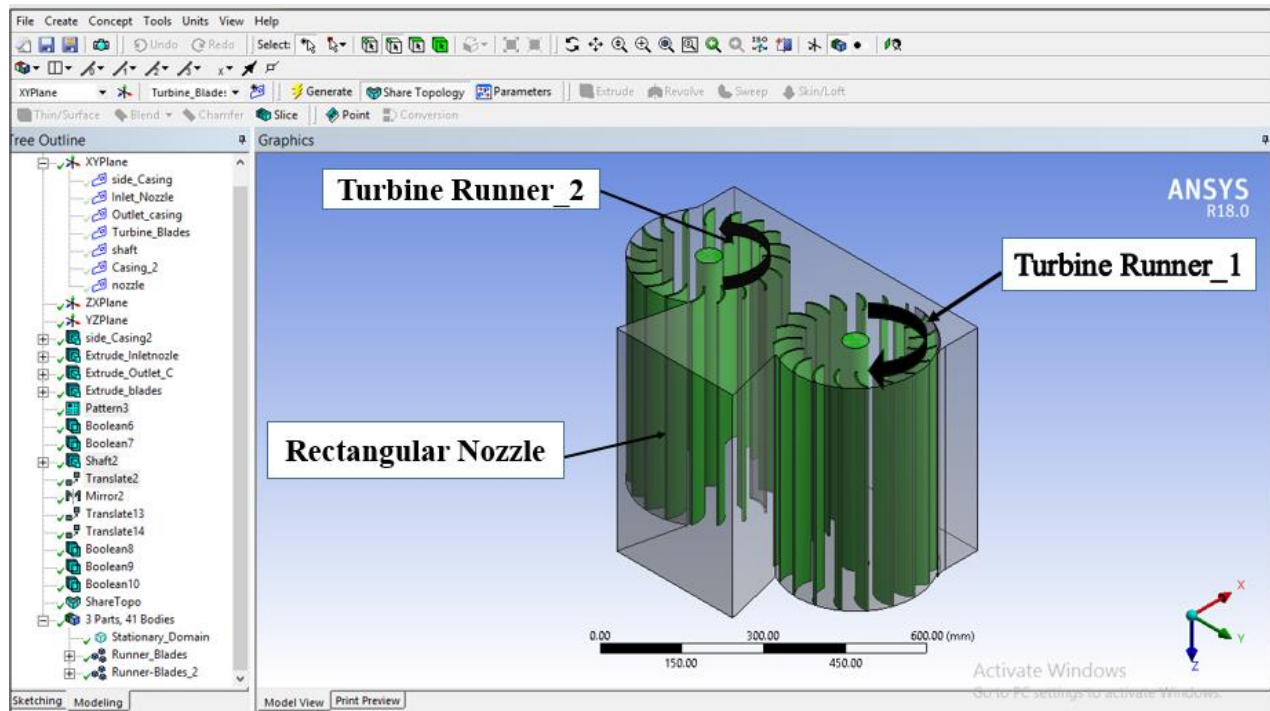


Figure 17: The 3D geometry of dual axis cross flow

Figure (17) shows the fluid domains of the casing and the runners of the turbine. This is a stationary fluid domain in which there will be flow of water at the given input velocity. Here, the inner wall of the fluid domain is defined as the interface between the runner and the casing. At this point, through which water is transacted and the rotational fluid domain is rotated at the given input (rpm). Here, the interface is the faces of the blades through which the water will be transferred from the casing to the runner fluid domain.

The rotating fluid domain consists of the turbine blades, the rotating walls adjacent to the turbine blades, and the central shaft; whereas, the stationary fluid domain consists of the inlet, the outlet, and the boundary walls associated with these regions. Additionally, the total fluid domain was split into two equal halves by using the symmetry tool in the ANSYS Design Modeler. Below, Figure (18) shows image of the rotating and stationary domains with the symmetry and stationary domain contains half of the flow inlet.

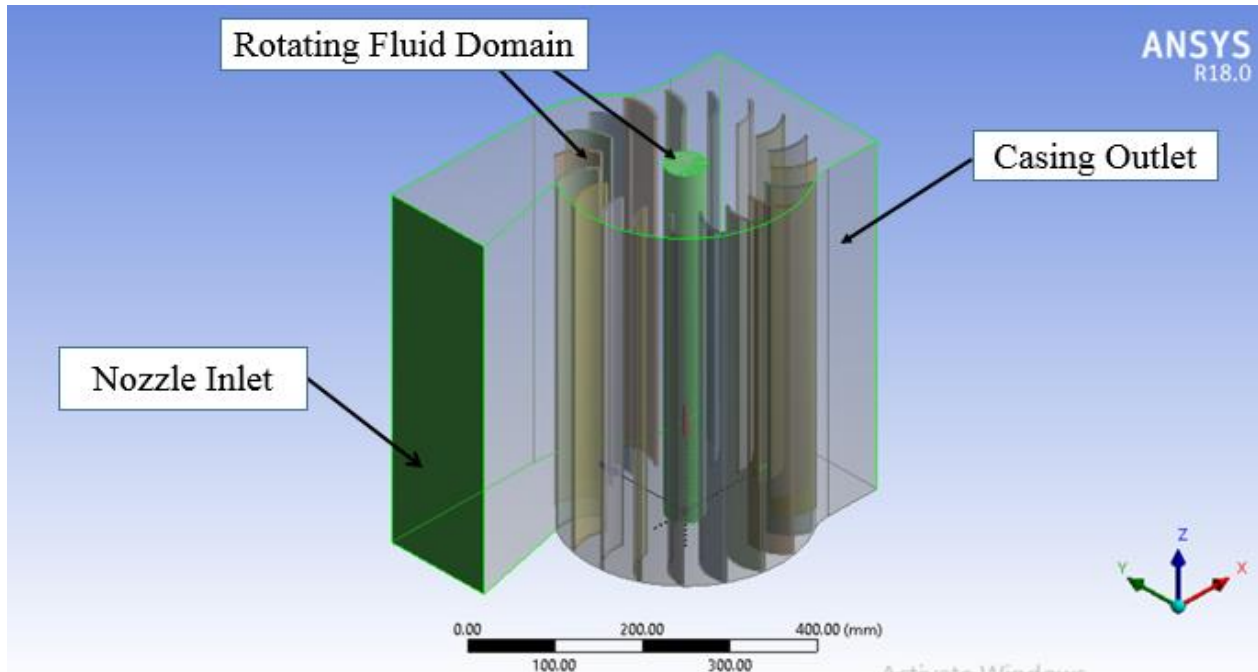


Figure 18: The 3D geometry for Numerical Analysis

The symmetry plane is parallel to both walls of the turbine casing and nozzle, and it passes exactly halfway between these two walls. The geometry is exactly symmetrical to this plane which reduces the volume of the fluid domain that must be part of the computational domain by a factor of two. This reduces the number of nodes and elements by factor of two solved by the ANSYS Fluent, and increases the computational speed by a factor of two. Finally, this symmetrical geometry from ANSYS Design Modeler is then imported into the ANSYS Meshing routine.

#### 4.12.2. Computational Mesh Generation

Meshing is an important step in any computational fluid dynamic simulation. To this end, ANSYS Meshing tool is used for discretizing the cross flow turbine geometry. The meshing is the differentiation of the components into very small sized elements of different shapes like triangular mesh, square mesh, hexagon mesh, tetrahedron mesh etc., which can be employed at different places of the component for the accuracy of the results. The accuracy of the results is based on the mesh quality and sizing. As the size of the mesh reduces, the accuracy of the result increases. However, the time for getting to that result increases. The software calculates the inlet and outlet parameters at the different faces of the mesh thereby generating accurate result. Further, in the area of higher gradients of analyzed parameters, higher grid density or finer

meshing can be used to obtain acceptable levels of solution accuracy, but it also increases the computation time. Another quality factor of the meshing is its skewness. The skewness is defined as the extent how the mesh shape is distorted. The lower the skewness, the higher is the quality of mesh. In the present case, relevance center has been selected as fine to ensure finer mesh, and the inflation is provided at the four places which are: At Casing – Runner Interface, the side face of the blades, the runner shaft face, and the front faces of the runner blades.

#### 4.12.2.1. Rotating Fluid Domain

The rotating domain consisted of 85996 mesh elements (58962 nodes). For a designed turbine runner with 18 blades and center shaft, the addition of inflation near the walls increases the number of elements from 85996 to 926166.

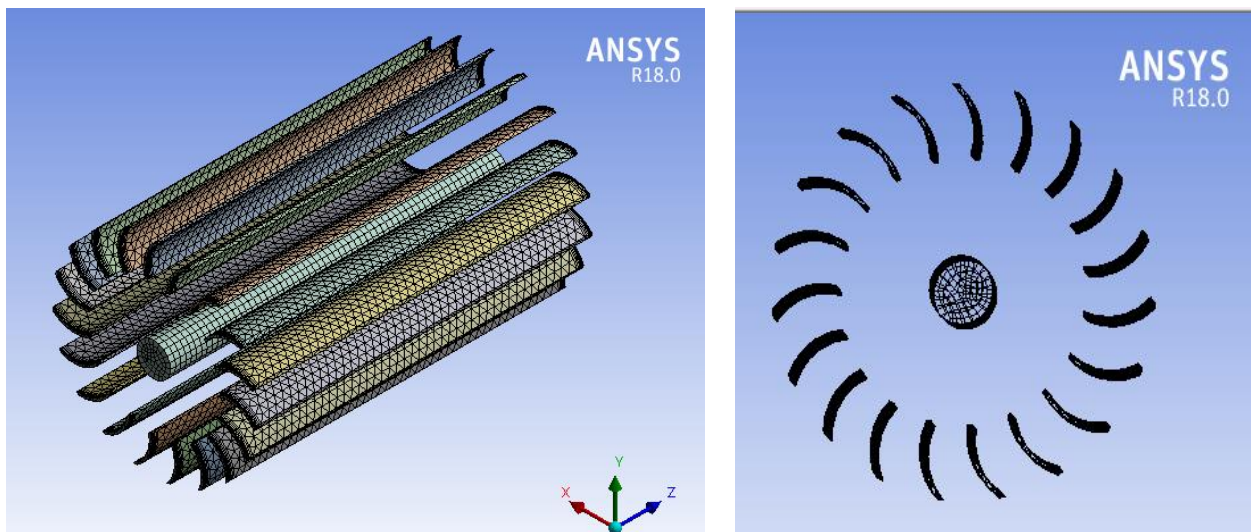


Figure 19: Computational mesh of the rotating domains

Further, the addition of inflation decreased the minimum orthogonal quality from 0.72 to 0.27 and increased the maximum skewness ratio from 0.84 to 0.9. Figure 19 shows the computational mesh of the rotating domains.

#### 4.12.2.3. Stationary Fluid Domain

The stationary domain consisted of 65942 mesh elements (43950 nodes). All the elements were hexahedral and the sizing was controlled depending on the flow direction that was easily predictable in this domain. The skewness factor describing the quality of a hexahedral mesh was kept below 0.8 and the maximum aspect ratio was 38. Figure (20) shows the computational mesh of the stationary domain.

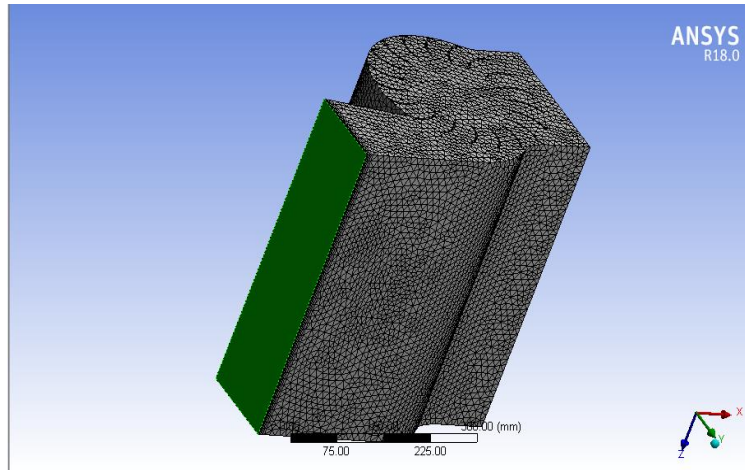


Figure 20: Mesh of the stationary domain with Nozzle inlet face.

### 4.12.3. Problem Solving Setup

#### 4.12.3.1. Assumptions

The following assumptions were made during the computational fluid dynamics simulation of cross flow turbine based on the literatures reviewed.:

- ✓ The fluid is three dimensional planar, turbulent.
- ✓ The fluid is a Newtonian, incompressible fluid.
- ✓ Double Precision, Segregated Steady Solver,
- ✓ Body forces are negligible.
- ✓ Fluid velocity on the casing walls are zero.
- ✓ No vapor is present in the water (single phase flow), and
- ✓ There is no leakage in the turbine and the surface of all the components is hydraulically smooth.

#### 4.12.3.2. Material Properties Database

The properties of the different solid and liquid materials are selected here for the model. The working fluid is chosen from the database in ANSYS and copied. The material chosen is water with constant default density and constant default viscosity corresponding to single phase flow. The values of density and viscosity for water are 998.2 kg/m<sup>3</sup> and 0.001003 kg/m-s, respectively, and water is selected as the material for the fluid part (as shown in Figure 21).

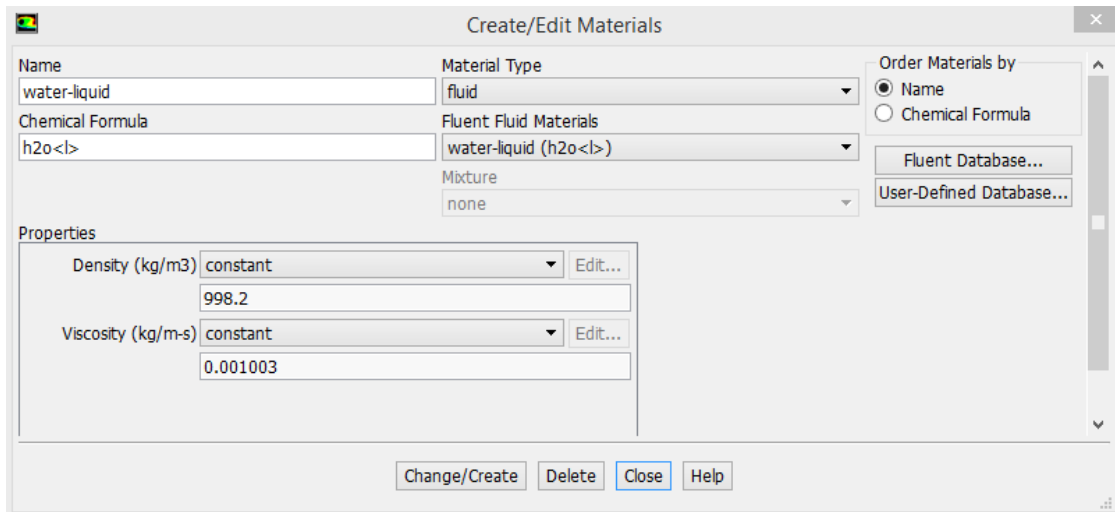


Figure 21: Selection of material

#### 4.12.3.3. Selection of the physical models

After selecting the analysis type, the solution and the turbulence model are specified. There are different types of turbulence models available in ANSYS Fluent 18.0. In present study, k-omega standard turbulence model is taken for analysis of the model.

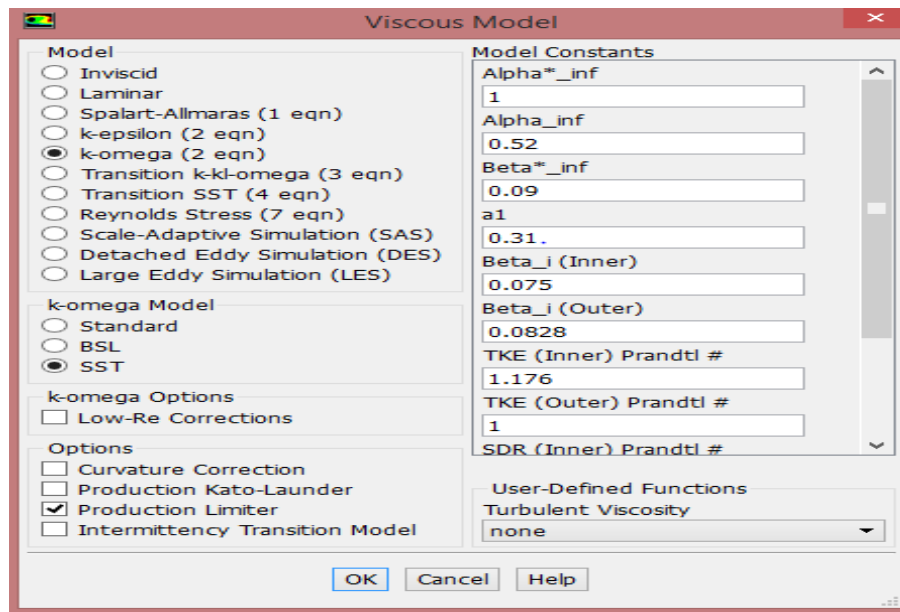


Figure 22: Selection of turbulence model

#### 4.12.3.4. Cell Zone Conditions Setup

In this setup, the condition of the zone, such as mesh motion, frame motion, porous zone, etc. is specified. In this study, the runner is the rotating part and, hence, frame motion feature is activated and given for the runner as the cell zone condition. A 375 rpm is assigned as the rotational velocity of the interior region along with the direction of rotation and the solid body is

rotating with the relative velocity of runner. The casing and nozzle are stationary so that no frame motion is given for these components. The cell zone setup for the runner is given below in Figure 23.

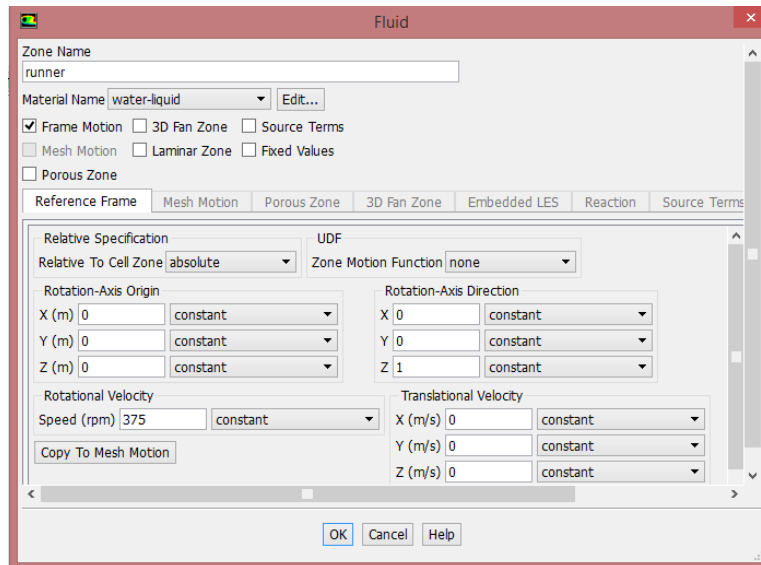


Figure 23: Cell Zone condition for runner.

#### 4.12.4. Boundary Conditions Set up

After the successful meshing of the modelled component, different inlet and outlet boundary conditions are given for the inlet and the outlet faces of the fluid domain. To solve the governing differential equations, they have to be closed by specifying boundary conditions. Defining boundary conditions involve identifying the locations of the boundaries (such as inlet, outlet, walls, etc.) as well as supplying the information at the boundary. In incompressible flow, the inlet total pressure and the static pressure are related to the inlet velocity by Bernoulli's equation. Hence, the velocity magnitude and the mass flow rate could be assigned at the inlet boundary. In the present study, the boundary conditions are specified as follows:

- ✓ Flow - material – water-liquid,
- ✓ Motion Type - moving reference frame with rotational speed (rpm),
- ✓ Inlet - inlet velocity of the fluid,
- ✓ Outlet - outlet pressure,
- ✓ Wall - stationary and moving wall, and
- ✓ Symmetric Boundary Conditions.



Therefore, the above specified conditions play a critical role in determining the final numerical output.

#### 4.12.4.1. Inlet Boundary Conditions

The inlet velocity boundary conditions were used to define the fluid velocity at the flow inlet. The magnitude of the inlet velocity is specified and the direction is taken to be normal to the boundary. In the current analysis, specifying the inlet fluid velocity at the nozzle is taken to be 7.2 m/s and the gage pressure at the inlet is taken to be zero. Assuming a turbulence intensity level of 5% and hydraulic diameter of 0.6m at the inlet specifies the turbulence parameters. ANSYS Fluent V18.0 has the following form for inlet velocity boundary conditions.

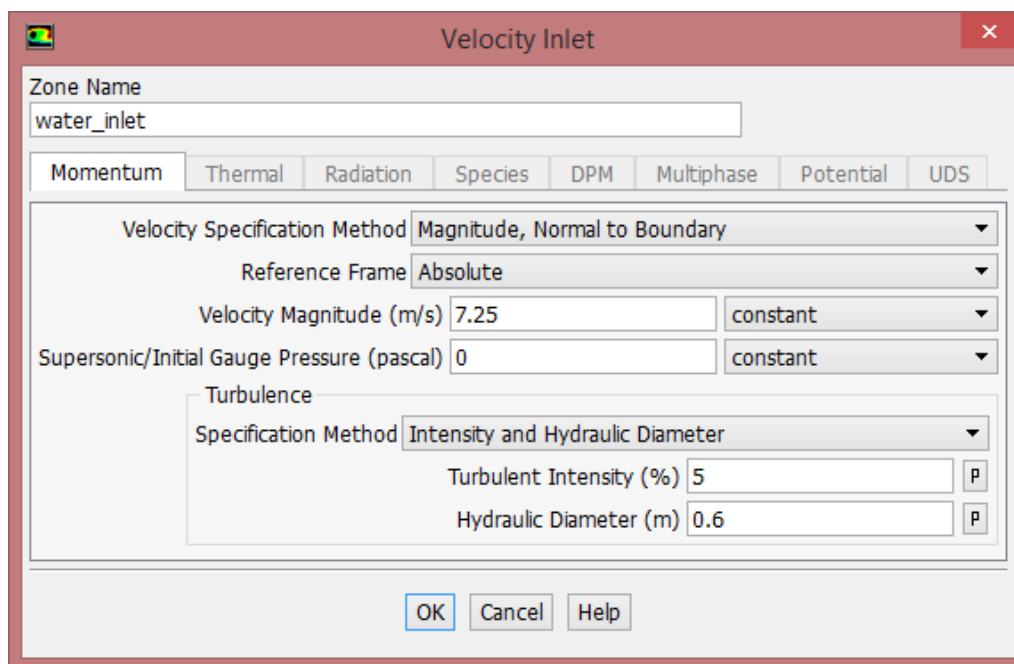


Figure 24: Inlet velocity boundary condition panel

#### 4.12.4.2. Outlet Boundary Conditions

The casing outlet face is described as pressure outlet boundary condition where the exit atmospheric pressure can be specified. In this boundary panel, the outlet boundary of the domain needs to satisfy the pressure distribution. Turbulent intensity is taken as 5% and hydraulic diameter as 0.8 m for outlet.

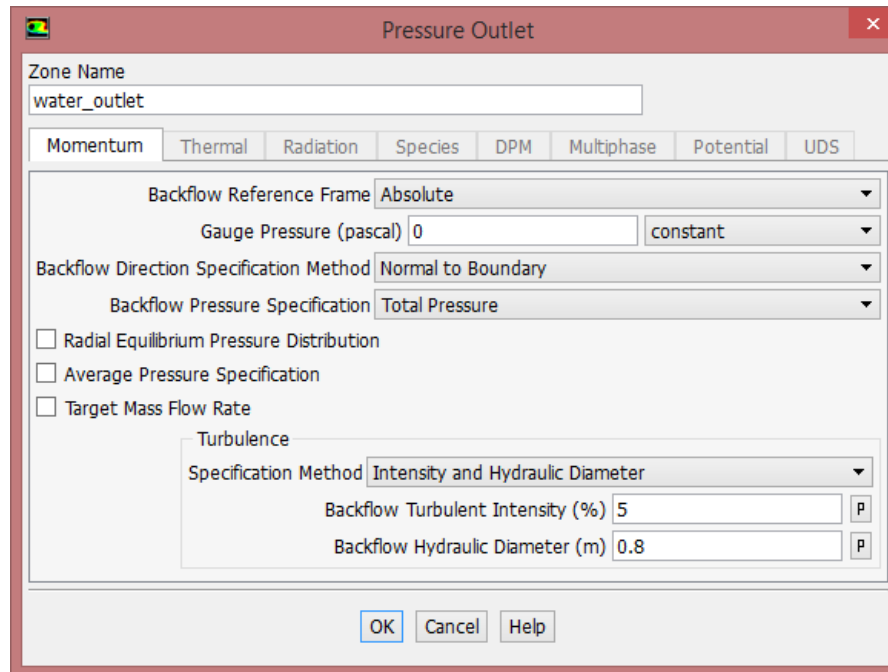


Figure 25: Outlet pressure boundary condition panel

#### 4.12.4.3. Symmetry Boundary Conditions

The symmetry boundary conditions are used when the physical geometry of interest and the expected pattern of the flow/thermal solution have mirror symmetry. They can also be used to model zero-shear slip walls in viscous flows. Symmetry boundaries are used to reduce the extent of the computational model to a symmetric subsection of the overall physical system.

#### 4.12.4.3. Wall Boundary Conditions

The wall boundary conditions are used to bound fluid and solid regions. In viscous flows, the no-slip boundary condition is enforced at walls by default, but one can specify a tangential velocity component in terms of the translational or rotational motion of the wall boundary, or model a slip wall by specifying shear. The shear stress between the fluid and wall are computed based on the flow details in the local flow field. In present study, runner, blades and solid bodies are specified as moving wall with rotational motion and no slip condition. The shaft of the turbine runner is defined as moving wall which rotates at a speed of zero relative to adjacent cell zone. The casing is also defined as a wall, but with zero absolute velocity. The boundary condition of runner walls is shown in the Figure (26).

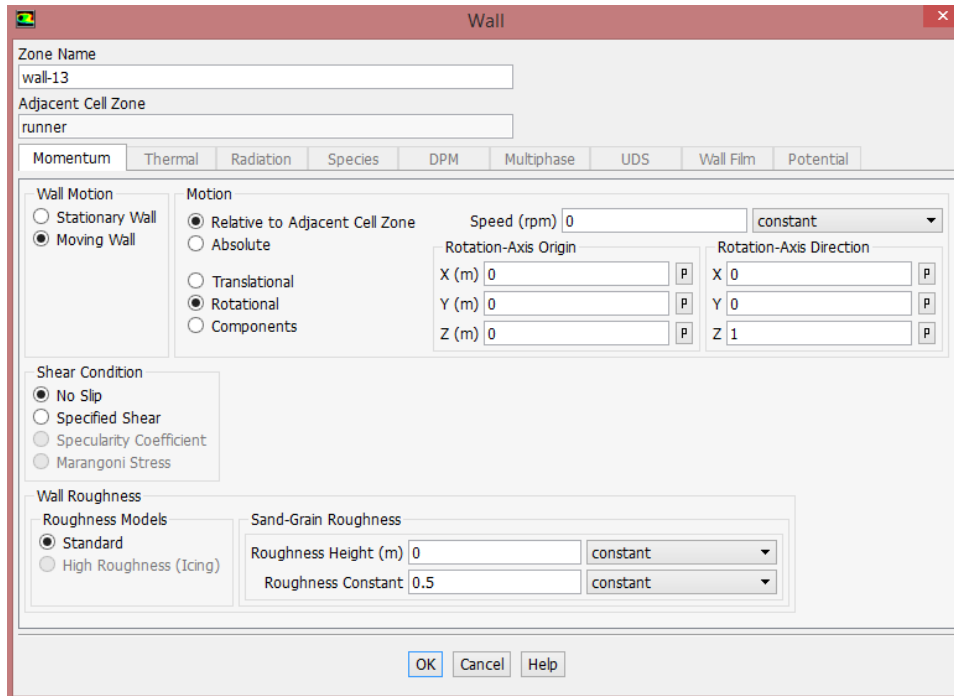


Figure 26: Boundary condition for runner wall

#### 4.12.5. Solution Method

For selection of algorithms (such as SIMPLE, SIMPLEC, PISO, etc.), the SIMPLE algorithm with Pressure-Velocity Coupling is selected for the present study. For the numerical solution of momentum, turbulence kinetic energy and turbulence dissipation rate equations, second order upwind discretization scheme is selected. Thus, second order upwind discretization is preferred for higher accuracy. The other things to be controlled for the solution are the under-relaxation factors. Because the non-linearity of the equation set is solved by the segregated solver, it is necessary to control the change of solution variables at each iteration, which is typically done by under-relaxation. If unstable or divergent behavior is observed, however, the under relaxation factors for pressure, momentum, and  $k$  from their default values may need to be reduced. Therefore, the solution controls under-relaxation factors for pressure, density, body forces, momentum, turbulent kinetic energy, specific dissipation rate and turbulent viscosity are equal to their default values of 0.3, 1, 1, 0.7, 0.8, 0.8, and 1, respectively.

#### 4.12.6. Solver Control

The residual monitors are set and the convergence criteria for continuity, x-velocity, y-velocity, z-velocity, and  $k$  are set at third decimal convergence of  $10^{-6}$ . The problem is now ready to be iterated and the number of iterations is specified and the reporting interval is set as one so as to

monitor the trend every time. The iteration continues till the convergence criteria in all the five parameters namely continuity, x, y, z velocity, and k are attained. Thus, the plot of the convergence can be viewed, simultaneously, by activating the display window.

#### **4.12.7. Solution Initialization**

The solution variable is initialized to eliminate any garbage before running the calculations. There are two methods available in ANSYS fluent package for the solution initialization, namely, Hybrid Initialization and Standard Initialization. For the present analysis, the Standard Initialization is chosen and the solution is initialized from inlet. Finally, the last step of the solver setup is to check all the settings and then specify the number of iterations.

## CHAPTER 5 RESULTS AND DISCUSSION

### 5.1. General

This chapter provides a discussion on the achieved computational fluid dynamics results. Moreover, the results of the analysis in ANSYS fluent can be shown by using graphical displays and numerical outputs. In general, the simulation using computational fluid dynamics tool is very important to understand the velocity and pressure distribution inside the nozzle, runner blades and turbine casing.

In the present study, the hydraulic performance of the designed ultra-low head cross flow turbine is simulated for the design rotational speed. Then, results of a number of rotational speeds higher than the design rotational speed are compared with the CFD analysis. After the successful input of the boundary conditions at the required faces, fluent solver is started for the calculations which determine the momentum and mass flow at each and every faces of the mesh generated earlier. In the ANSYS Fluent analysis, the values of various output parameters such as moment, pressure contour, velocity contour, velocity vector, streamlines are also obtained and finally, it is followed by the analysis of the results.

### 5.2. Graphical Display

The overall flow pattern in cross flow turbines can be clearly seen in graphical displays. The necessary graphical displays for flow in cross flow turbine are velocity vector colored by velocity magnitude, contour of static and total pressure, and contour of velocity magnitude, which are shown below.

#### 5.2.1. Pressure Distribution on the Cross Flow Turbine

The operating conditions for the simulations were set to standard atmospheric temperature and pressure. The pressure contours show the variation of pressures along the cross flow turbine. It is observed that pressure decreases as it passes through the nozzle exit and further decreases when it strikes the turbine blades and the value of the pressure remains constant at entire part of the runner as shown in Figure (27). Although temperature is not simulated, the only minor fluctuations in pressure are noticed; pressure is tracked in a detailed manner. Since the fluid flow properties like density does not change with application of pressure, it is affected with hydraulic head. In general, the flow is assumed to be isothermal. Figure (27) shows the variation of pressure in the pressure contours. The figure (27) clearly shows the regions of high pressure at inlet section of the rectangular nozzle. This indicates that the velocities at this section are low and the pressure

distribution gradually goes on decreasing along the length of the nozzle at which are the water velocities are high and the pressures are low and vice versa.

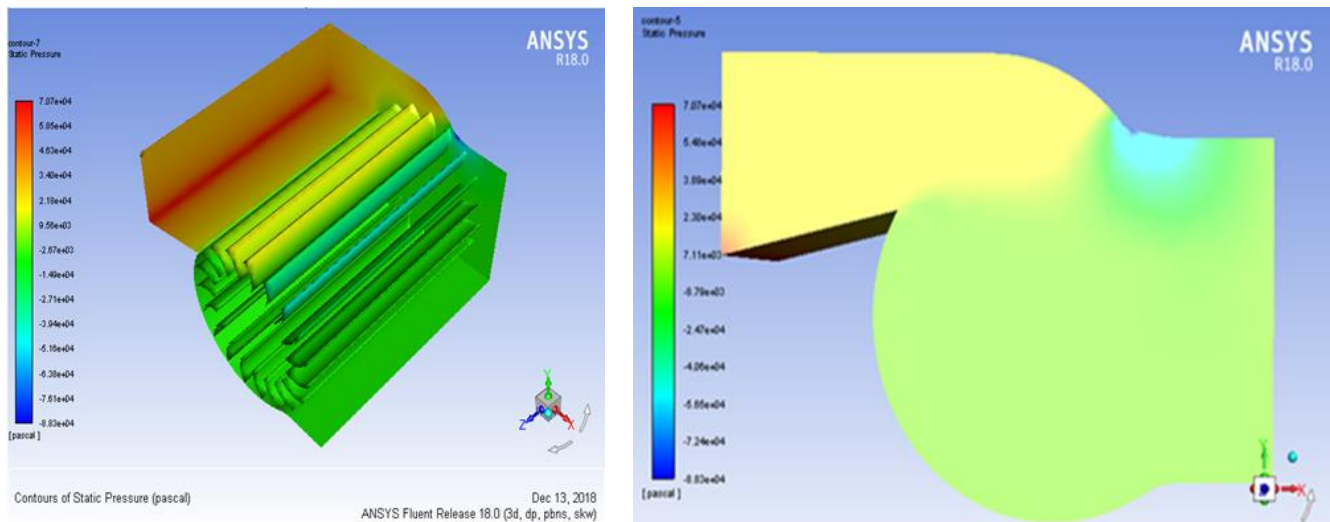


Figure 27: The contours of static pressure

From figure 27, as the fluid color goes from red to deep blue, the static pressure magnitude goes from the maximum to the minimum and it can even be negative at the region where there is no cross flow. Further, the variation of total pressure at the runner blades is shown in figure 28.

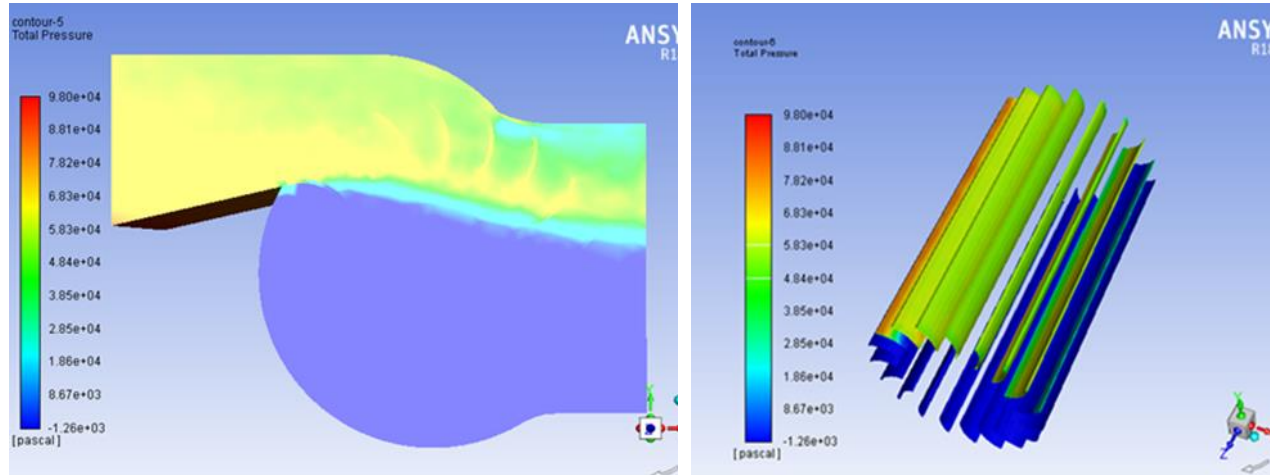


Figure 28: Displays the contours of total pressure on the blades.

From figure 28, it can be observed that maximum pressure occurs at the inlet of nozzles compared to turbine exit. It clearly shows that the maximum energy has been transferred at the first stage of the turbine. Then, it is going to decrease at the second stage and at the outlet of the turbine. Therefore, the pressure variation is mainly caused due to hydraulic head and flow of water through different configurations.

### 5.2.2. Velocity Vectors and Velocity Distributions

Figure 29 shows the velocity contours of the flow in the cross flow turbine. The velocities with different magnitudes are shown by the different colors and are depicted in the legend shown on the left side of the figure. Velocities in the nozzle and internal area of the runner are changed obviously by the change of the nozzle shape. In the case of nozzle shape at the exit, the water velocity in the rectangular nozzle passage becomes higher than that of the inlet. As a whole, fluid velocity becomes accelerated along the contracted nozzle passage from the inlet. The velocity of water in the nozzle inlet and outlet are analytically calculated to be 7.25m/sec and 12.9m/sec, respectively. However, this values need to be compared with computational fluid dynamics simulation results. The values of the fluid velocity do not remain constant at all parts of the cross flow turbine. Figure 29 clearly shows that the highest velocities in the flow are at the exit region of turbine nozzle where the velocity vectors are red in color.

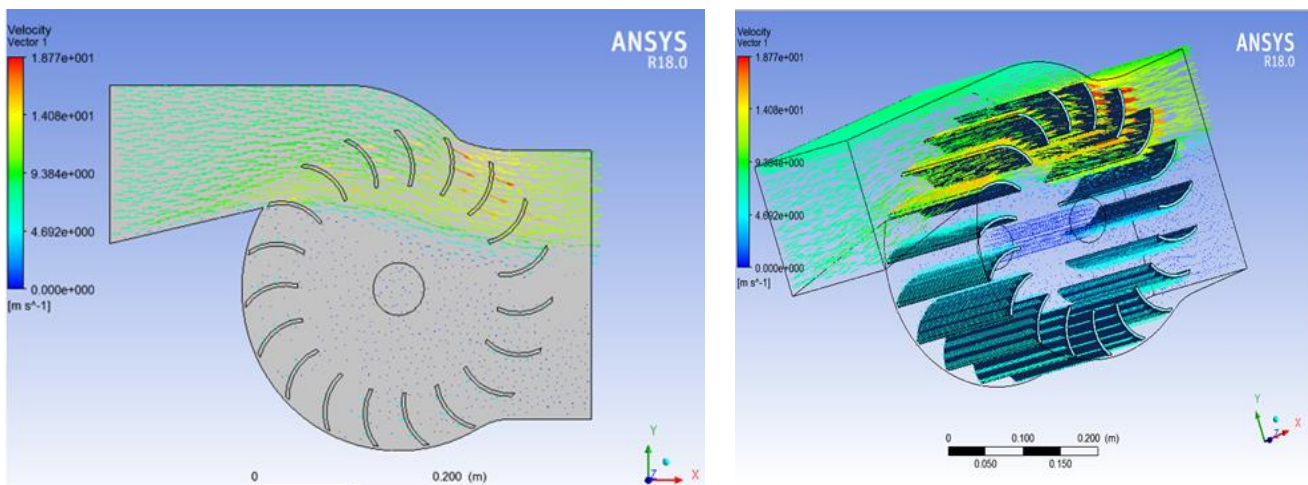


Figure 29: Velocity distribution of cross flow turbine

The flow velocity at the inlet of the nozzle is constant, and it is going to increase inside the nozzle near at the first stage of turbine blades and then going to decrease at the second stage outlet of the turbine runner. The theoretical water jet velocity comes out to be 12.9m/sec, whereas the numerical jet velocity is at 18.77m/sec, the fluid travels an empty space of about 3mm, which is the distance between the nozzle and the runner. Then, this jet velocity strikes the lower portion of the turbine blade, and it is going to decrease at the turbine exit section. From figure 29, it can be observed that the inlet velocity condition was 12.9 m/s while the maximum velocity in the flow domain was found to be 18.77m/s.

### 5.3. The Numerical Hydraulic Efficiency Comparison

In this study, hydraulic efficiency of ultra-low head cross flow turbine under different rotational speed of runner has been worked out as shown in figure 30. For the purpose of comparison, plots of turbine efficiency are made as a function of runner rotational speed. The general parabolic shape of the efficiency versus rotational speed curve is typical of ultra-low head CFTs. To prepare these plots, time consuming CFD simulations had to be done at several turbine rotational speeds. Each turbine rotational speed required around 8 to 12 hours of computer CPU time. In this process of the simulation, the rotational speeds of shaft within the turbine runner are taken in increasing order from 150 to 900rpm. All the hydraulic turbine efficiencies in this curve were calculated numerically using the torque acting on the runner times the angular rotational speed and dividing it by the product of water flowrate and total pressure (Pascal) at nozzle inlet and turbine runner outlet, which are taken from the Fluent result and substituted in equation 4.6.

The hydraulic performance of the designed ultra-low head cross flow turbine is simulated for the design rotational speed and a number of increased rotational speeds higher than the design rotational speed, results of which are compared with the similitude analysis.

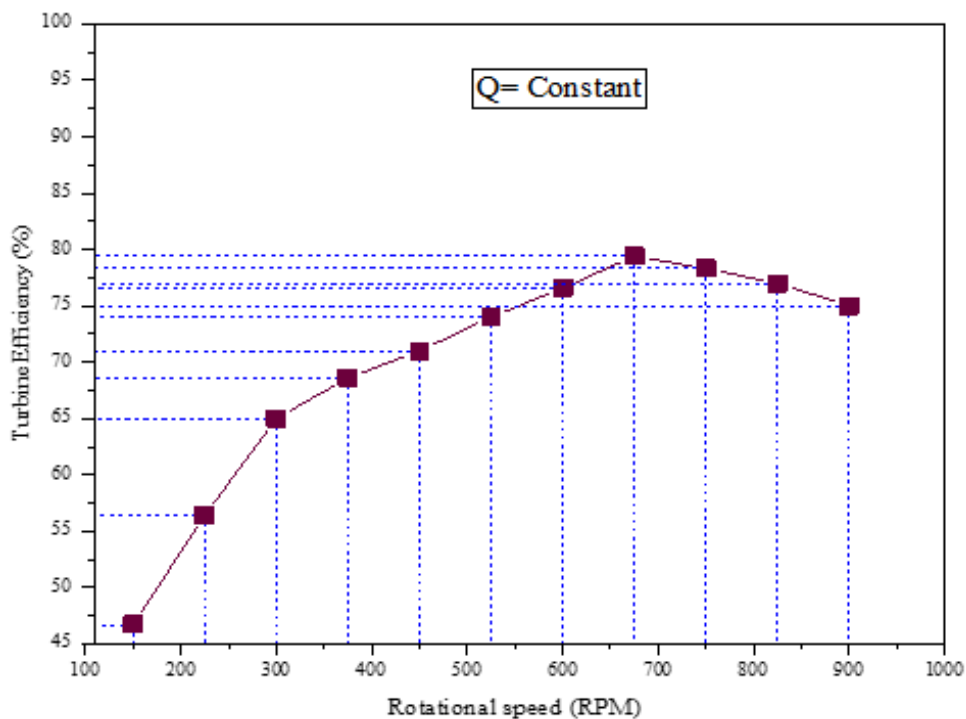


Figure 30: Turbine performance curves as a function of rotational speed



Figure 30 shows the variation of Efficiency vs. rotational speed of turbine runner. According to figure 30, the efficiency is maximum at 675rpm and beyond this value of speed, it is observed that the efficiency is dropped as the rotational speed is increased.

As it can be seen from the above figure 30,hydraulic efficiency at a rotational speed of 675rpm is 78%, which is the optimum point and the operating range from 600 to 825 rpm provides very good performance. Further, the efficiency gradually increased from 46.68% to 78% with the increase of rotational speed from 150 to 675rpm and the efficiency decreased as the speed is increased from 750 to 900 rpm. The results obtained showed that, at the designed water flow rate and head, efficiency of the turbine was improved from 67.5% to 78% (increase by 10.5%) numerically, whereas the analytical analysis were found as 87.9%.

## **CHAPTER 6 CONCLUSIONS AND RECOMMENDATIONS**

This is the final chapter that summaries the outcomes of the research and reflects on the goals set. Recommendations for the future work are also provided in this chapter.

### **6.1. Conclusions**

The overall study methodology adopted for this research work includes analytical studies and Computational fluid dynamics simulation.

The first part of this paper, data collection including measurements like head and flow rate, which accounts 2.65m and 1.02m<sup>3</sup>/s respectively were conducted. Then, design analysis of ultra-low head cross flow turbine for the case of Wonji-Shoa Sugar factory irrigation canal flow based on the collected data was carried out. These design parameters such as, turbine power, runner outer and inner diameter, water jet thickness, number of blades, blade spacing and blade profile were determined at maximum turbine efficiency. In addition to this, there were a few more consideration that are found essential for a micro hydropower scheme including, nozzle with rectangular cross-sectional area and speed multiplying mechanism of spur gear which increase the rotational speed of turbine runner from 375rpm to 1500rpm to drive the standard generator, is also designed.

The second part of this thesis work, Computational Fluid Dynamics (CFD) modeling of nozzle, runner and turbine casing were carried out using ANSYS Fluent v18.0. The 3D geometry was also modeled on ANSYS Design modeler workbench. Subsequently, the model was imported to ANSYS-Fluent to visualize the flow characteristics over the nozzle and runner blades. This ANSYS Fluent CFD analysis, provides velocity vector and pressure contour in the flow passage are displayed and hence, visualizing and understanding the internal fluid flow in the cross flow turbine is easily possible. These plots are all taken at the symmetric cross sectional plane of the turbine.

Additionally, simulations were carried out using viscous, RANS equations, steady state with SST  $k-\omega$  turbulence model, rotating frame of reference, including the effects of rotational speed (rpm) were also performed. The results showed that hydraulic efficiency obtained with CFD analysis and analytical approaches were found as 78% and 87.9%, respectively, which shows that the values are close to each other.

## **6.2. Recommendations**

Furthermore, the following recommendation can be addressed for the future research work in the field of micro hydropower schemes for rural electrification in the developing countries.

- ✓ In the present CFD analysis, flow is assumed to be steady state. In the future study, unsteady flow analysis can be carried out.
- ✓ The hydraulic performance of the ultra-low head dual axis cross flow turbine can be evaluated experimentally and the results should be compared with those of the CFD analysis to conclude that the turbine meets the design requirements.
- ✓ Lastly, it is recommended that Wonji-Shoa Sugar Factory can support the present finding with experimental results and install a prototype in the sugar factory irrigation canal flow.

## REFERENCES

- [1]. International Energy Agency, (2017, April 16).
- [2]. World Energy Council, “Survey of Energy Resources”, Technical Report, Sep.2013.
- [3]. International Journal of Energy and Environment Volume 5, Issue 2, 2014 pp.155-182, Journal homepage: [www.IJEE.IEEFoundation.org](http://www.IJEE.IEEFoundation.org)
- [4]. "World small hydropower development report 2016," United Nations Industrial Development Organization and the International Center on Small Hydro Power, Vienna, May. 2017.
- [5]. mnre.gov.in [accessed on 10 April. 2016].
- [6]. International Course on Small Hydropower Development, February 2004, by AHEC, IITR
- [7]. Addis Ababa University(AAU) 2014. Feasibility study on Potential Power Capacity Assessment for Ultra-Low Head Micro Hydropower Sites in Ethiopia, Addis Ababa, Ethiopia.
- [8]. Melessaw Shanko, Ethiopia’s Small Hydro Energy Market Target Market Analysis, December 2009 [www.renewables-made-in-germany.com](http://www.renewables-made-in-germany.com)
- [9]. Pokhrel, Sajjan. M.S.R.C.E. Department of Mechanical and Materials Engineering, Wright State University, 2017. Computational Modeling of a Williams Cross Flow Turbine
- [110]. Paul Breeze. Power Generation Technology. Elsevier, Linacre House, Jordan Hill, Oxford OX2 8DP, 2005.
- [11]. Shin-Ichi Inage. Prospects for Large-Scale Energy Storage in Decarbonized Power Grids. International Energy Agency, 9 rue de la Federation 75739 Paris Cedex 15, France, 2009.
- [12]. Hydroelectric Power: How it works, USGS Water Science for Schools, (2011) from <http://ga.water.usgs.gov/edu/hyhowworks.html>
- [13]. Helena Ramos. Guidelines for Design of Small Hydropower Plants. WREAN (Western Regional Energy Agency & Network), Belfast, North Ireland, 2000
- [14]. Daniel A. N. —A Guide to hydropower| canyon hydro Inc. pp 1-24
- [15]. Benzon, D., Aggidis, G. A., and Anagnostopoulos, J. (2016). Development of the turgo impulse turbine: Past and present. Applied Energy, 166:1–18
- [16]. Sinagra, M., Sammartano, V., Aric`o, C., Collura, A., and Tucciarelli, T. (2014). Cross-flow turbine design for variable operating conditions. Procedia Engineering, 70:1539–1548.

- [17]. Elbatran, A., Yaakob, O., Ahmed, Y. M., and Shabara, H. (2015). Operation, performance and economic analysis of low head micro-hydropower turbines for rural and remote areas: a review. *Renewable and Sustainable Energy Reviews*, 43:40–50.
- [18]. Paul Breeze. *Power Generation Technology*. Elsevier, Linacre House, Jordan Hill, Oxford OX2 8DP, 2005.
- [19] Helena Ramos. *Guidelines for Design of Small Hydropower Plants*. WREAN (Western Regional Energy Agency & Network), Belfast, North Ireland, 2000.
- [20]. Shepherd, D. G. (1956). *Principles of turbomachinery*. Macmillan.
- [21] NPTEL Mechanical Engineering Faculty. Impulse turbine, lecture 26. Online, June 2015.
- [22] European Small Hydropower Association. *Guide on How to Develop a Small Hydropower Plant*. European Renewable Energy Council, Belgium, 2004.
- [23] David Kilama Okot. Review of small hydropower technology. *Renewable and Sustainable EnergyReview*, 26:515–520, 2013.
- [24]. Pereira.N.H & Borges.J.E; “Study of the nozzle flow in a Cross flow turbine”; *Int. J. Mech. Sci.*, Vol.38, No. 3, pp. 283-302 (1996).
- [25]. Paish O. (2001) —Micro-hydropower: status and prospects|| SPECIAL ISSUE PAPER Proc Instn Mach Engrs Vol 216 Part A: J Power and Energy pp 31-40
- [26]. [www.eee.ntu.ac.uk/research/microhydro](http://www.eee.ntu.ac.uk/research/microhydro)
- [27]. Jim Norman” Got water, need power” ABS Alaskan, Inc
- [28]. Neil J., Jian K., Steve S., Abigail H. and Papatya D. (2011), —Acoustic impact of an urban micro hydro scheme|| World Renewable Energy Congress – Sweden 8–13 May, 2011 Linköping, Sweden. p1448
- [29]. —Hydropower Micro-Systems, A buyer ‘s guide|| natural resources Canada pp 1-53
- [30] Paish Oliver. Small hydro power: technology and current status. *Renewable and Sustainable Energy Reviews*, 6(6):537–556, 2002.
- [31] Selection of Generator Type, available from <http://waterturbines.wikidot.com/system:join>
- [32]. Shimokawa K, Furukawa A, Okuma K, Matsushita D, Watanabe S. Experimental study on simplification of Darrius-type hydro turbine with inlet nozzle for extra low head hydropower utilization. *Renew Energy* 2012; 41:376–82.

- [33]. Hothersall, R. A review of the cross-flow turbine. In *Waterpower '85*, Proceedings of the International Conference on Hydropower, Las Vegas, NV, USA, 25–27 September 1985; ASCE: New York, NY, USA, 1985.
- [34]. Chappell, J. R., “Recent DOE-Sponsored Hydropower Engineering Research”, Report No. ECG-M-02983, p6, 1983.
- [35]. Adhau SP, Moharil RM, Adhau PG. Mini-hydro power generation on existing irrigation projects: case study of Indian sites. *Renew Sustain Energy Rev* 2012; 16:4785–95.
- [36]. Khosrowpanah S, Fiuzat AA, and Albertson ML. Experimental study of cross flow turbine. *J. Hydraulic. Eng.*, 114. 299-314; 1988.
- [37]. Vincenzo, Costanza, Armando, Oreste and Tullio. Banki-Michell. Optimal Design by Computational Fluid Dynamics Testing and Hydrodynamic Analysis, *energies* 2013, ISSN 1996-1073.
- [38]. Nadim M. Aziz and V. R. Desai, “An Experimental Study of the Effect of Some Design Parameters in Cross-Flow Turbine Efficiency”, Engineering Report, Department of Civil Engineering, Clemson University, 1993.
- [39]. Nakase, Y., Fukutomi, J., Wantanabe, T., Suessugu, T., and Kubota, T., “A study of Crossflow Turbine”, *Small Hydro Power Fluid Machinery*, p. 13-18, 1982.
- [40]. H. Olgun (1998). “Investigation of the performance of a cross-flow turbine.” *International Journal of energy Research*, 22(11), 953-964.
- [41]. Eve Cathrin Walseth, *Practical Implementations of Computational Fluid Dynamics in the Design Practice - Virtual Hydraulic Laboratory*, Conference materials, Hydro forum 2000, Czorsztyn, Poland.
- [42]. Chiyembekezo S. Kaunda<sup>1</sup>, Cuthbert Z. Kimambo<sup>2</sup>, Torbjorn K. Nielsen<sup>1</sup>,” A numerical investigation of flow profile and performance of a low cost Crossflow turbine” *International Energy and Environment Foundation* (2014).
- [43]. Jesus De Andrade, Christian Curiel, Frank Kenyery, Orlando Anguillón, Auristela Vásquez, and Miguel Asuaje. “Numerical investigation of the internal flow in a banki turbine.” *International Journal of Rotating Machinery* (2011).
- [44]. Sammartano, V.; Aricò, C.; Carravetta, A.; Fecarotta, O.; Tucciarelli, T. Banki-Michell optimal design by computational fluid dynamics testing and hydrodynamic analysis. *Energies* 2013, 6, 2362–2385.

- [45]. Bhutta, S.M. Technology and information of small scale hydel power. Proceeding of the International Conference about Hydel Power Development in Pakistan. University of Engineering and Technology, Taxila, Pakistan, 2008.
- [46]. Nebiyu Bogale Mereke, Highly Efficient Cross Flow Turbine Runner Design for Upgrading Traditional Water Mill in to Micro Hydro Power Plant (A case Study for Kersa-Minko Village), International Journal of Engineering and Technical Research, Vol. 4 Issue 12, December-2015.
- [47]. Fiuzat, A.A. and B.P. Akerkar, The use of interior guide tube in cross flow turbines. Proceeding of the International Conference on Hydropower (WaterPower, 89). London, UK. 1989.
- [48]. Csanady, G. T., Theory of Turbomachines, McGraw-Hill Book Co., New York, USA, pp. 122, 1964.
- [49]. Dixon, S. L., Fluid Mechanics and Thermodynamics of Turbomachinery, 4th ed., Butterworth-Heinemann, Boston, pp. 145, 1998.
- [50]. Spur Gears. [cited 2017; Available from:  
[http://www.roymech.co.uk/Useful\\_Tables/Drive/Gears.html](http://www.roymech.co.uk/Useful_Tables/Drive/Gears.html).
- [51]. “Design Data Hand Book for Mechanical Engineers” By K. Mahadevan & K. Balaveera Reddy
- [52]. Shigley, J.E. and Uicker, J.J., Theory of machines and mechanisms, McGraw-Hill, 1986.
- [53]. Dynamic loads on gear tooth. Buckingham, Earle. New York: ASME Research publication, 1931.
- [54]. Versteeg, H.K., and Malalasekera, W., “An Introduction to Computational Fluid Dynamics”, First edition (2005), Longman Scientific & Technical Publication
- [55]. Ferziger, J.H. and Peric, M., “Computational Methods for Fluid Dynamics” 3<sup>rd</sup> edition-revised (2004).

## APPENDIX

### APPENDIX A

Questioner for wonji/shoa sugar factory irrigation department and irrigation canals workers at wonji/shoa site.

**Date:** \_\_\_\_\_

**Site Location:** \_\_\_\_\_

**Contact Name:** \_\_\_\_\_ **Contact Phone:** \_\_\_\_\_ **Contact email:** \_\_\_\_\_

The measurements were carried to address the following questions:

1. What are the sources of water for Wonji-Shoa Sugar factory? \_\_\_\_\_
  - A, Is there storage/Dam?
  - B, The design discharge of liters per second (l/sec). \_\_\_\_\_
2. The water is drawn from River using gravity diversion or a pumping station. \_\_\_\_\_
  - A, what is the total volume of water that is taken from the river per day? \_\_\_\_\_
  - B, the water diverted from the river is 24 or less than 24 hours per day.
3. What is the structure of the canal?
  - I. A rectangular or Trapezoidal shape.
  - II. The construction of a permanent or temporary weir.
4. The width and the height of the canal vary in different locations. **Yes, No**
5. What is the design discharge of the canal or the actual total canal capacity? \_\_\_\_\_
6. The Water supply in the canal is sufficient for irrigation during the dry season. **Yes, NO**
7. What is the average flow or volume in the canal irrigation networks per day? \_\_\_\_\_
8. The volume of water conveyed through this canal for irrigation during the day or at night.
9. The dry season is during the months of February, March, April and May, when the volume decreases to an average of (m<sup>3</sup>/sec). \_\_\_\_\_



10. The discharge in the stream fluctuates following the rainfall pattern and peaks during the months of July, August, September and October, with the volume averaging a maximum peak of (m<sup>3</sup>/sec). \_\_\_\_\_
11. Depending on the season, these systems require cleaning and monitoring by the operator. Who flushes out and removes the obstructing particles such as stones sand leaves?
12. Were the measured Irrigation water flow data through canals at various location available or not available?
13. Is there the data of the annual water supply to Wonji/Shoa sugar factory for irrigation & Steam power plant?
14. Are there suitable sites for MHP (i.e. Related to available head, Flow rate)?
15. Population size or villagers living near by the canal.
16. Do the villagers have access to electricity
17. Is there available head in the canal?
18. Is there the sugar factory background data available or not available?

**APPENDIX B****RECEIVING WATER FLOW INFORMATION**

Date of measurement: \_\_\_\_\_

Data source: \_\_\_\_\_

Measurement Location (e.g. closest road /crossing): \_\_\_\_\_

Latitude/Longitude (optional): \_\_\_\_\_

How to Estimate Flow



Table 1:Hydrological measurements at the case-study Wonji/Shoa Sugar Factory

Trial	Width of Canal(m)	Depth(m)	Area(m <sup>2</sup> ) (Width X depth)	Floating distance(m)	Time(sec)	Velocity(m/s)
1						
2						
3						
4						
5						

**FLOAT METHOD**

**Equipment Needed:**Measuring tape, Timer (stopwatch), Float (Tennis ball), Paper and pencil for record keeping.

Average time (Sec): \_\_\_\_\_, Average Canal depth (m): \_\_\_\_\_, Average Canal Width (m): \_\_\_\_\_

Estimated flow rate (m<sup>3</sup>/s): \_\_\_\_\_





